GEOLOGIJA 69/1, 55-76, Ljubljana 2026
© Author(s) 2026. CC Atribution 4.0 License

https://doi.org/10.5474/geologija.2026.003
Article

Multiple controllers on organic matter accumulation at the Mesopotamia Basin of the Chia Gara Formation shale, Central Iraq

Dejavniki, ki nadzorujejo kopičenje organske snovi v skrilavcih formacije Chia Gara v Mezopotamskem bazenu v osrednjem Iraku

Rana A. ALI[1]* & Iman A. AL-ALI[2]

[1,2]Department of Geology, College of Science, University of Baghdad, Iraq;
[1]*corresponding author: rana.ali@sc.uobaghdad.edu.iq

Prejeto / Received 22. 4. 2025; Sprejeto / Accepted 27. 2. 2026; Objavljeno na spletu / Published online 7. 4. 2026

Key words: Mo isotopes, redox conditions, organic matter, primary productivity, geochemical methods, Upper Jurassic–Early Cretaceous, Mesopotamian Basin
Ključne besede: Izotopi Mo, redoks pogoji, organska snov, primarna produktivnost, geokemične metode, zgornja jura–spodnja kreda, Mezopotamski bazen

Abstract

The Tithonian–Berriasian Chia Gara Formation in Central Iraq represents a major breakthrough in shale oil exploration. This study investigates two continuous core sections (140 m and 137 m) from the East Baghdad (EB1) and Balad (Ba1) oilfields, located within the intrashelf basin along the passive margin of the Arabian Plate. Comprehensive geochemical analyses, including major and trace elements, Mo isotopes, and total organic carbon (TOC), were conducted to evaluate the mechanisms controlling organic matter enrichment. The EB1 and Ba1 cores are subdivided into five and four organic sedimentary facies (OSF), respectively. In EB1, TOC values in the lower OSF 1 and OSF2 range from 3.55 to 8.0 wt.% and 2.31 to 4.42 wt.% and are higher than those of the upper OSF 3, OSF 4, and OSF 5 that range from 0.5 to 3.77 wt. %. In Ba1, OSF 3 and OSF 5, which range from 0.39 to 2.7 wt.%. Redox indicators such as U/Th, Ni/Co, EF(U), and EF(Mo) show a progressive shift towards more oxic bottom-water conditions. The $\delta^{98/95}$Mo data (– 0.3 to 2.5 ‰) confirm the presence of euxinic conditions, particularly within OSF2 in both EB1 and Ba1, thereby resolving previous uncertainties regarding bottom-water redox conditions. Primary productivity indices (Cu/Al and Ni/Al ratios) suggest relatively low productivity in deep-water slope and basinal facies. Furthermore, the upwelling indicators (EF(Co) × EF(Mn)), varying from 0 to 0.48 for EB1 and 0.05 to 0.18 for Ba1, suggest that preservation conditions played a more significant role than productivity conditions within the deep-water slope and basin. Differential subsidence, with local uplifts and erosion within the Mesopotamian Foredeep Basin likely contributed to spatial variability in organic enrichment. Overall, this study highlights the importance of the redox environment in the development of high-quality hydrocarbon source rocks in unrestricted environments that present upwelling.

Izvleček

Titonijsko–berriasijska formacija Chia Gara v osrednjem Iraku predstavlja pomemben preboj pri raziskovanju nafte iz skrilavcev. Študija obravnava dva neprekinjena jedrna odseka (140 m in 137 m) z naftnih polj East Baghdad (EB1) in Balad (Ba1), ki se nahajata v znotrajšelfnem bazenu ob pasivnem robu Arabske plošče. Opravljene so bile obsežne geokemične analize, vključno z določitvijo glavnih in slednih elementov, izotopov Mo ter skupnega organskega ogljika (TOC), z namenom opredelitve mehanizmov, ki nadzorujejo obogatitev z organsko snovjo. Jedri EB1 in Ba1 sta razdeljeni v pet oziroma štiri organske sedimentne faciese (OSF). V jedru EB1 se vrednosti TOC v spodnjih OSF1 in OSF2 gibljejo med 3,55 in 8,0 ut. % ter 2,31 in 4,42 ut. %, kar je višje kot v zgornjih OSF3, OSF4 in OSF5 (0,5 do 3,77 ut. %). V jedru Ba1 so vrednosti TOC v OSF3 in OSF5 med 0,39 in 2,7 ut. %. Redoks kazalniki, kot so U/Th, Ni/Co, EF(U) in EF(Mo), kažejo postopen premik proti bolj oksidacijskim razmeram na dnu vodnega stolpca. Podatki $\delta^{98/95}$Mo (–0.3 do 2.5 ‰) potrjujejo prisotnost evksiničnih razmer, zlasti v OSF2, kar odpravlja prejšnje nejasnosti glede redoks pogojev pri dnu. Kazalnika primarne produktivnosti (razmerji Cu/Al in Ni/Al) nakazujeta razmeroma nizko produktivnost v globokovodnih pobočnih in bazenskih faciesih, medtem ko kazalniki dviganja globokovodnih vod (EF(Co) × EF(Mn)), ki se gibljejo med 0 in 0,48 za EB1 ter med 0,05 in 0,18 za Ba1, kažejo, da so pogoji ohranjanja imeli večji vpliv kot produktivnost. Diferencialno pogrezanje, skupaj z lokalnimi dvigi in erozijo v Mezopotamskem predgorskem bazenu, je verjetno vplivalo na prostorsko variabilnost obogatitve z organsko snovjo. Študija tako poudarja ključno vlogo redoks okolja pri nastanku kakovostnih izvornih kamnin za ogljikovodike v odprtih okoljih z značilnim dviganjem globokovodnih vod.

Introduction

During the Tithonian–Berriasian transition, dramatic changes occurred in oceanography, biology, and geochemistry (Lodowski et al., 2024). Jurassic–early Cretaceous black shales provide an important record of this period and offer valuable important insights into the marine environment and the emergence of life (Langrock et al., 2003). Organic matter (OM) accumulates primarily through two models: a preservation model mainly regulated by redox conditions (Chen et al., 2023), as seen in the present Black Sea, and a productivity model, mainly influenced by high productivity (Lu et al., 2019), as in the modern Arabian Sea. OM enrichment in marine shale is influenced by anoxic conditions and high palaeoproductivity (Lin et al., 2024). Additionally, low energy environment and greater input of organic matter than inorganic mineral substances are required. Numerous studies have shown that terrigenous input, changes in circulation patterns, and water mass restrictions also impact OM enrichment (Zhang et al., 2023; Li et al., 2024; Shen et al., 2024; Lu et al., 2025). Recent research suggest that redox conditions and productivity are likely two of several factors influencing OM enrichment in shale, with potentially distinct regulatory mechanisms in different environmental settings (Zhang et al., 2023).

During periods of transgression and global sea level fluctuations, the Tithonian–Berriasian Chia Gara Formation's black shale and carbonate were extensively deposited in Central Iraq during the Upper Jurassic–Cretaceous (Al-Ameri, 2011). This period produced good source rocks due to the

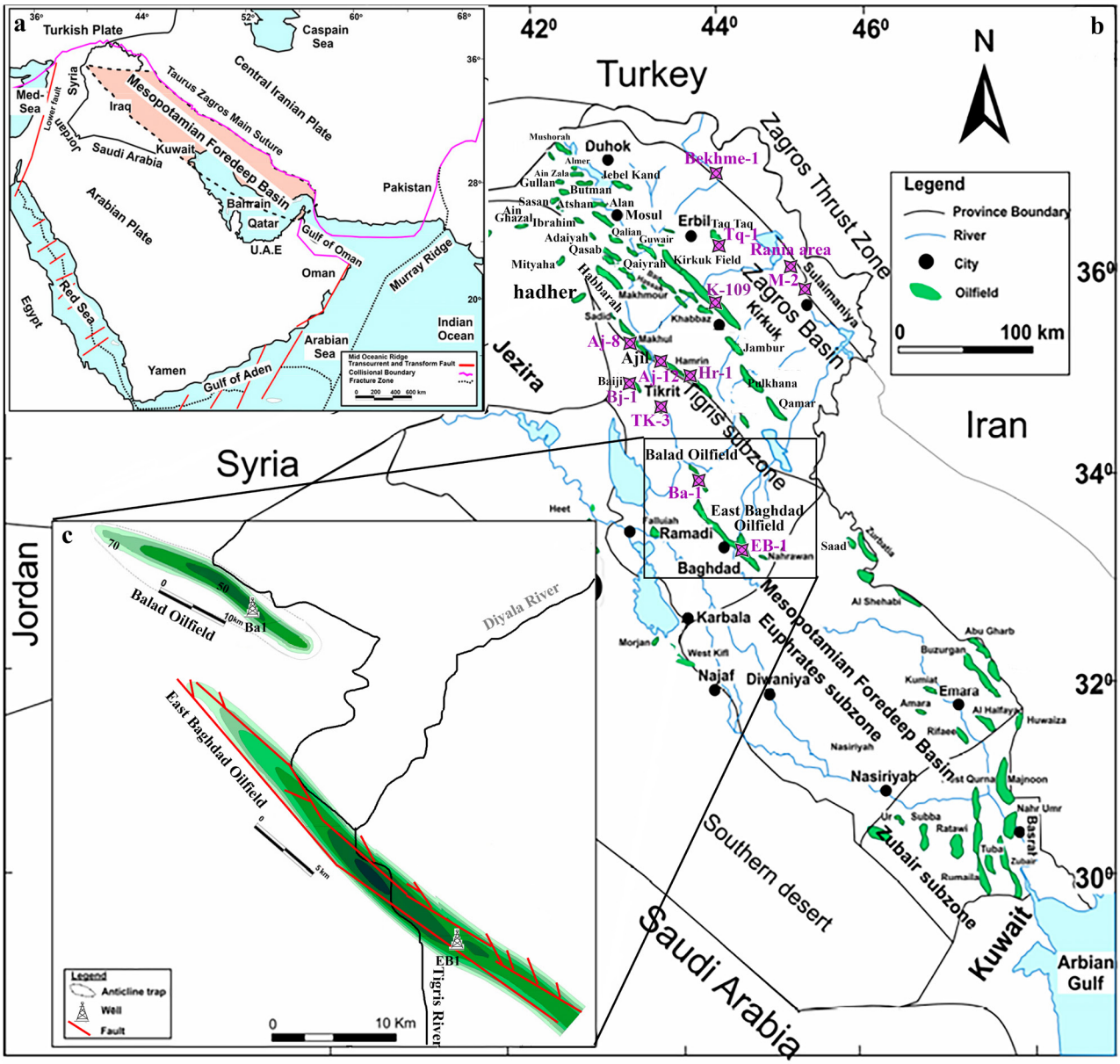

Fig. 1. (a) The Mesopotamian Basin and the main structural divisions of Iraqi territory are shown on the location map of the research area; (b & c) inset location maps of the East Baghdad and Balad Oilfields and the oil wells under investigation.

global warming and the deposition of shale, and carbonate rock. Since the Mesozoic Era, Central Iraq has been an ideal site for marine deposition (Edilbi & Sherwani, 2019). Large but shallow intrashelf basins formed on the passive margins of the Arabian Plate (Fig. 1a, b), and the Neo-Tethys Ocean at this time due to slow subsidence. Previous studies based on borehole analysis and outcrop profiles have documented episodes of economic upwelling and sea level changes, influencing both carbonate platform facies and deep-water slope and basinal facies (Al-Beyati et al., 2021). A widespread hiatus in the earliest Cretaceous is thought to be due to differential subsidence with local uplifts and erosion in the Mesopotamian Basin in Central Iraq, which led to upwelling.

These events altered the region's primary productivity and water column redox conditions, further affecting OM enrichment (Mohialdeen & Hakimi, 2016). However, it remains unknown weather upwelling occurred in the intrashelf basin area compared to other thoroughly studied areas of Central Iraq. Good-quality hydrocarbon source rocks from the Upper Jurassic-Cretaceous period accumulated in the facies of intrashelf basin, as evidenced by the discovery of the East Baghdad and Balad Oilfields (Fig. 1c), which have high hydrocarbon recoveries. Previous research indicates that the shale of the Chia Gara Formation in the Mesopotamian Foredeep Basin and northern Iraq was deposited in an anoxic environment devoid of euxinic (oxygen-depleted and enriched with H_2S) bottom water, due to the absence of sedimentary iron species studies and Ni-Mo sulphide deposits in the cores (Al-Ameri, 2011; Al-Ameri et al., 2012a & b). On the other hand, other studies suggest that North Iraq has euxinic bottom water (Mohialdeen & Raza, 2013; Al-Jaafary, 2015). Therefore, the process of OM enrichment during the sedimentation of the Chia Gara Formation in the Mesopotamian Foredeep Basin, as well as the main controlling parameters for OM enrichment in region with the lowest high total organic carbon (TOC), are still unknown.

The continuous wells EB1 and Ba1 (Fig. 2a, b), located in the central region of the Mesopotamian Basin on the Arabian Plate Margins, central Iraq, were subject to comprehensive analyses of total organic carbon (TOC) content, geochemistry (major and trace elements), and isotopic composition, with a focus on $\delta^{98}/^{95}$Mo in this study. The aim was to reconstruct the redox state of bottom waters and primary productivity during the deposition of Upper Jurassic–Cretaceous Chia Gara Formation shale (Fig. 1b) in the East Baghdad and Balad Oilfields in the central Mesopotamian Basin. Additionally, it sought to clarify the main controlling factors and enrichment processes responsible for OM accumulation in various facies.

Geological Background

The study area consists of the East Baghdad and Balad Oilfields (Fig. 1a, b, c), located within the Mesopotamian Fore Deep Basin and belong to the Arabian Basin at the regional scale. These two locations are situated within the Arabian Peninsula Basins, with a focus on the northeastern Iraqi region of Arabian Peninsula's. The East Baghdad Oilfield is situated in the middle of Iraq, approximately 10 kilometers east of Baghdad. Its coordinates are 33° 21' 4.79" N latitude and 44° 38' 31.79" E longitude. The field covers an area roughly 20–30 km wide and 120 km long (Al-Ameri et al., 2016; Ali & Jassim, 2023; Ali, 2023). Structurally, the East Baghdad oil field may grade northeast towards the Zagross Fold Belt and westward towards the boundary of the Widian Basin of the Interior Platform.

The Balad Oilfield, located at latitude 34° 00' 53.46" N, and longitude 44° 08' 44.66" E, is located in the Unfolded Zone (Fig. 1a, b, c), approximately 9 km from Balad city and 60–70 km north of Baghdad in the Salah Al-Deen urban area. The formation of the Zagros anticlines in Iraq resulted from subtle deformation just above a detachment at the lower boundary of the Palaeozoic succession, combined with more rigid twisting involving the basement. The elongated, asymmetrical anticlines in the Balad Oilfield, separated by narrowing synclines, may be controlled by thrust faults (McQuarrie, 2004).

During the Late Cretaceous, the Arabian Plate and continental blocks of Eurasia collided, forming the Mesopotamian Basin as a NW-trending foredeep. The Mesopotamian Basin, which contains Tethys Ocean deposits from the Jurassic and Cretaceous periods, extends southward. Due to tectonic instability and mostly oxygen-depleted palaeoenvironments near the equator, the Arabian Region's largest oil and gas reserves developed, and high organic matter was preserved. From the Jurassic, through the Cretaceous and Palaeogene, up to the Middle Miocene Fatha Anhydrite, the generalised lithostratigraphic section consists of marine and subordinate lagoon beds deposited in the southern Tethys Ocean as sediments of shales, carbonates, and anhydrites. It has mild folding and a graben-horst structure that is 100 km long, expanding NW-SE of the Baghdad urban region (Simmons et al., 2007). The Chia Gara Formation

was deposited in a large intra-shelf basin in the Arabian Plate's Late Tithonian–Turonian mega-sequence (AP8), coinciding with a new phase of ocean floor expansion.

Al-Beyati (1998) identified organic sedimentary facies (OSF) in the Chia Gara Formation, with five OSF in well EB1 (4570–4430 m) and four in well Ba1 (4095–3958 m) from top to bottom. The geochemical data from this study, together with previously defined sequence boundaries, are used to identify these organic sedimentary facies (OSF) in the Chia Gara Formation. These facies, along with their depths and petrographic descriptions, are summarised in Table 1 and Fig. 2 a & b.

Table 1. Organic sedimentary facies, depths, and rock descriptions of the Chia Gara Formation in the EB1 and Ba1 wells.

Depth [m] (East Baghdad Oilfield EB1)	Depth [m] (Balad Oilfield Ba1)	Organic sedimentary facies (OSF)	Rock description
4566–4570; 4532–5454; 4465–4471	4091–4095; 4009–4017; 3994–4004	OSF. 1	Consist of a low-hardness, slightly fissile, pyritic brown calcareous shale with amorphous type II kerogen and high TOC content.
4545–4566; 4471–4481	4078–4091; 4017–4026	OSF. 2	Consist of black shale with high pyritic content, is highly fissile, has high TOC content, and contains type II amorphous kerogen.
4494–4532; 4430–4461	4026–4078; 3958–3994	OSF. 3	It is predominantly composed of laminated shale and dark greenish--grey to blackish–grey argillaceous limestone, non-fissile, with high pyrite content, low TOC content, and type II amorphous kerogen.
4481–4494	-	OSF. 4	It is primarily composed of shining brown limestone, free of pyrite, with a medium TOC level, and containing only type II amorphous kerogen.
4461–4465	4004–4009	OSF. 5	Mostly consisting of brown limestone facies, which form part of the previous facies, these are quite similar to the host rock of the earlier facies, except for a slightly lower TOC content.

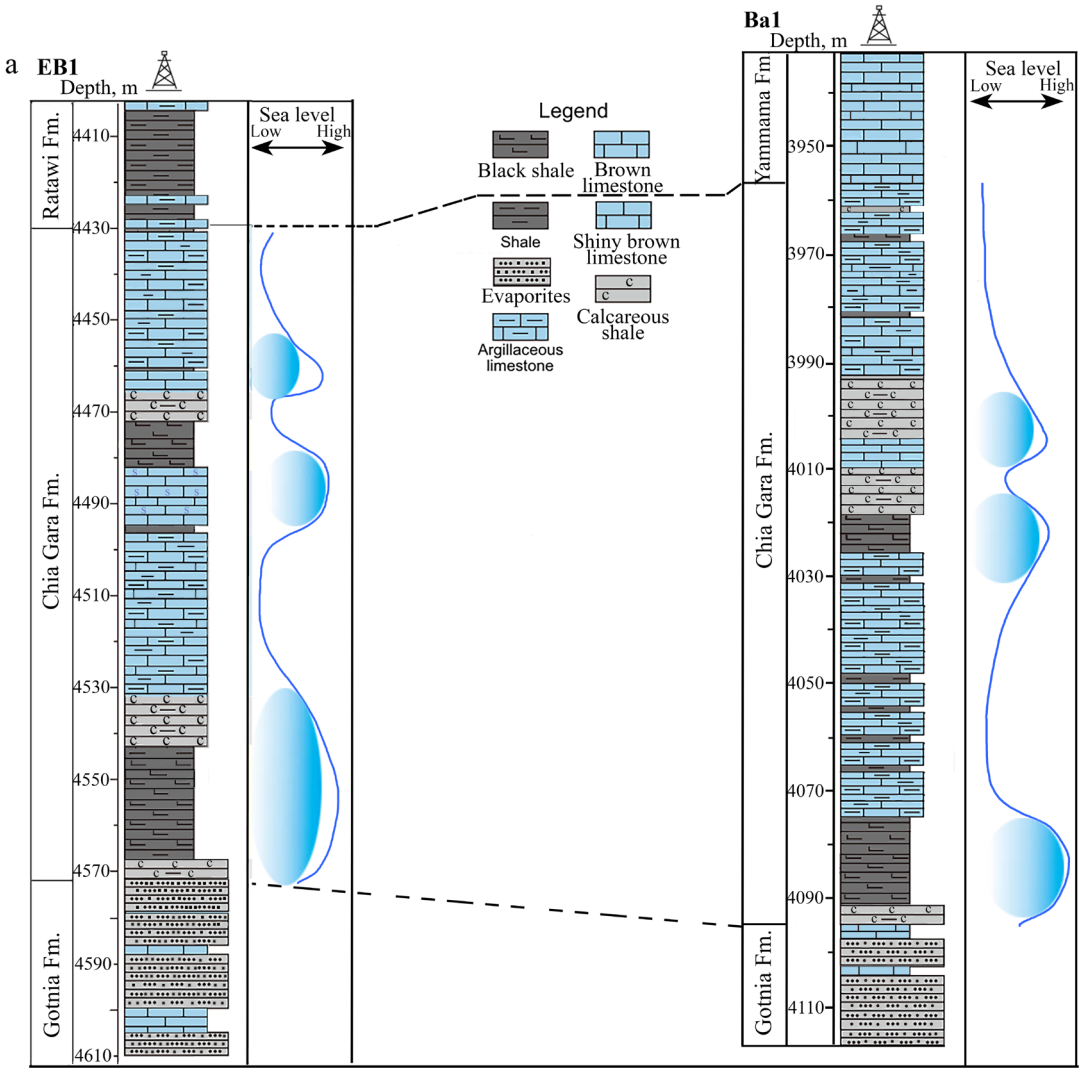

Fig. 2. Chia Gara Formation stratigraphic column with proportional sea level variations (a) in the EB1 well and (b) in the Ba1 well.

Materials and Methods

In the EB1 and Ba1 wells (Figs. 1 & 2), systematic sampling of the Chia Gara Formation was carried out based on the lithology and depth of the targeted interval. Mo isotope analysis, TOC analysis, and major and trace element analysis were performed on a total of thirty-two samples from both wells. Figures 1 and 2 show the site and depth of sample collection. To ensure the validity of the results, samples containing visible veins or nodules were removed prior to geochemical analysis. The remaining sample material was then manually pulverised using an agate mortar until it reached a size of 200 mesh.

Total organic carbon (TOC)

First, 10 % hydrochloric acid was added to the 200-mesh powder samples to remove the carbonate. The samples were then washed with distilled water to remove any remaining hydrochloric acid. After drying overnight, the samples were analysed using the CHNOS Elemental Analyser (Vario EL III, Germany).

Major and Trace Elements

The Panalytical Axios sequential X-ray fluorescence (XRF) spectrometer (Malvern Panalytical, UK) was used to analyse the major elements (SiO_2, Al_2O_3, Fe_2O_3, CaO, MgO, Na_2O, K_2O, TiO_2, P_2O_5) in the samples. The processed powder sample was combined in a ratio of 1:3:10 with oxidant (NH_3NO_3) and flux ($LiBO_2$, LiF, $Li_2B_4O_7$). For the XRF test, glass slices were heated in a furnace at 1150°C for 15 minutes. The contents of selected trace elements (V, Sc, Cr, Co, Ni, Cu, Zn, Mo, Rb, Sr, Ba, Th, U, Y, Zr, Nb, Hf, Cd) were determined using an Inductively Coupled Plasma–Mass Spectrometer (ICP–MS; PerkinElmer Nexion300D). Sample were digested in a mixture of hydrofluoric and nitric acid (HF–HNO_3, 1:3) at 185 °C for 24 hours to ensure complete dissolution. The resulting solution was then analysed by ICP–MS, yielding an accuracy of over ±5 %.

To evaluate the degree of enrichment with trace elements, enrichment factors (EF) were calculated following McLennan (2001). The EF was determined using the following equation:

$$X_{EF} = [(X/Al)_{sample}/(X/Al)_{PAAS}] \quad (1)$$

where the X stands for the specified trace element. The element X to Al weight ratio in the study sample is indicated by the subscript sample, while the Post Archean Australian Shale standard is indicated by PAAS. Values of $X_{EF} > 1.0$ or < 1.0 indicate element enrichment or depletion, respectively (Taylor & McLennan, 1985).

Isotopic Compositions of Mo ($\delta^{98/95}$Mo)

A suitable quantity of ^{97}Mo–^{100}Mo double spikes was applied to the sample according to the double-spike method (Li et al., 2014), taking into account the Mo content of the sample. After the sample's dissolution and purification of the sample with HCl, HNO_3, and HF at 130 °C, column separation was performed. MC-ICP-MS was used to determine the pure Mo, using ion-exchange chromatography with BPHA resin. The procedures of Siebert et al. (2001) and Zhao et al. (2016) were followed to correct for the double spike and normalise the data to the standard NIST-SRM-3134. The $\delta^{98/95}$Mo values of IAPSO seawater and NIST–SRM–3134 standard solutions were simultaneously and repeatedly evaluated throughout the analytical process. The two observed $\delta^{98/95}$Mo values are 0.00 ± 0.05 ‰ and 2.05 ± 0.07 ‰, respectively, which are consistent with published and verified values (Greber et al., 2012; Zhao et al. 2016; Nan et al., 2023). Meanwhile, the total Mo content in the samples was significantly higher than the Mo procedure the blank value (< 0.2 ng). Finally, the $\delta^{98/95}$Mo values for each sample were recalculated using the NIST–SRM–3134 recommended reference solution to ensure global comparability and accuracy.

The formula used to calculate the corrected $\delta^{98/95}$Mo values was:

$$\delta^{98/95}Mo_{auth} = [(\delta^{98/95}Mo_{tot} \times Mo_{tot} - \delta^{98/95}Mo_{det} \times Mo_{det})/Mo_{auth}] \quad (2)$$

where Mo_{det} = [(Mo/Al)PAAS × Al_{tot}] (PAAS= Post-Archean Australian Shale), this yielded the detrital Mo content (Mo_{det}) (Pearce et al., 2010), $Mo_{auth} = Mo_{tot} - Mo_{det}$ was used to calculate the authigenic Mo content. The contents of Al and Mo in PAAS (10 % and 1.0 mg/kg, respectively) and $\delta^{98/95}Mo_{det}$ value of 0.4 ‰ were used for detritus adjustment (Taylor & McLennan, 1985). $2\sigma x^2$ is equivalent to twice the standard deviation.

Table 2. Oil shale ratios and sedimentary features of the Chia Gara Formation in the EB1 and Ba1 wells.

Oilfield	Samples	Depth (m)	Organic sedimentary facies (OSF)	TOC (%)	$\delta^{98/95}$Mo (‰)	U/Th	Ni/Co	Cu/Al	Ni/Al	Ti/Al	Sr/Cu	Rb/Sr	EF(U)	EF(Mo)	EF(Mo)/EF(U)	Mo/TOC (mg/Kg/wt%)	Sedimentary features
East Baghdad	EBc_1	4437	OSF3	1.85	0.59	0.8	7.17	4×10^{-3}	8.1×10^{-3}	0.13	2.21	0.29	9.22	108.88	11.8	26.48	Regressive facies, hot and dry climate, increased organic production, poor ventilation, dysoxic conditions.
	EBc_2	4445	OSF3	0.5	0.61	0.85	7.64	2×10^{-3}	3.7×10^{-3}	0.19	2.7	0.3	5.9	42.82	7.25	74	
	EBc_3	4457	OSF3	1.74	– 0.1	0.88	6.15	2.7×10^{-3}	7.6×10^{-3}	0.1	3.2	0.36	10.43	71.89	6.89	18.96	
	EBc_4	4461	OSF5	2.2	1.11	1.78	7.94	3.15×10^{-3}	6.08×10^{-3}	0.15	2.71	0.28	11.40	286.03	25.09	64.21	Transgressive facies, hot and dry climate, low organic production, suboxic conditions.
	EBc_5	4464	OSF5	1.9	1.17	1.54	6.5	3.3×10^{-3}	5.9×10^{-3}	0.16	2.73	0.29	10.45	185.69	17.77	54	
	EBc_6	4465	OSF5	2.5	1.09	1.84	7.36	3.1×10^{-3}	5.57×10^{-3}	0.17	2.52	0.31	10.66	268.92	25.22	57.72	
	EBc_7	4470	OSF1	5.75	1.59	2.42	9.21	3.9×10^{-3}	9.95×10^{-3}	0.13	2.74	0.33	15.29	242.56	15.86	26.95	Regressive facies, hot and dry climate, decreased organic production, anoxic- to suboxic conditions.
	EBc_8	4472	OSF2	8.0	2.5	4.51	10.3	3.9×10^{-3}	9.5×10^{-3}	0.15	2.83	0.46	15.95	287.39	18.01	30.5	Sea level rise at the top, deep progressive facies, extreme reducing conditions, and elevated organic production, and euxinic conditions.
	EBc_9	4480	OSF2	7.87	2.09	3.53	13.88	2.6×10^{-3}	6.3×10^{-3}	0.14	3.4	0.4	12.28	186.12	15.15	27.95	
	EBc_{10}	4485	OSF4	3.77	1.00	1.64	7.26	3.0×10^{-3}	5.2×10^{-3}	0.13	2.6	0.27	9.60	169.21	17.62	35.27	Progressive facies, hot and dry tropical climate, suboxic conditions.
	EBc_{11}	4493	OSF4	2.95	1.35	1.88	7.35	2.9×10^{-3}	5.7×10^{-3}	0.129	2.7	0.24	9.2	169.29	18.4	43.72	
	EBc_{12}	4509	OSF3	1.9	– 0.25	0.76	7.46	1.4×10^{-3}	3.4×10^{-3}	0.11	3.6	0.19	4.0	46.58	11.64	23.68	Regressive facies, tropical climate, shallow basin, moderate organic production, poor ventilation, dysoxic conditions.
	EBc_{13}	4527	OSF3	1.84	0.54	0.84	7.75	1.7×10^{-3}	6.5×10^{-3}	0.13	3.09	0.15	8.06	36.84	4.57	11.41	
	EBc_{14}	4533	OSF1	4.52	1.51	2.56	10.8	4.1×10^{-3}	1×10^{-2}	0.16	2.9	0.23	19.23	254.9	13.25	31.63	Regressive facies, increased basin shallowness, low organic production, anoxic to suboxic conditions.
	EBc_{15}	4541	OSF1	3.55	1.67	2.52	11.7	2.4×10^{-3}	5.9×10^{-3}	0.08	3.44	0.31	11.13	128.96	11.58	36.62	
	EBc_{16}	4549	OSF2	6.74	2.33	5.59	15.54	2.9×10^{-3}	9.3×10^{-3}	0.09	3.64	0.35	12.1	231	19.1	37.53	Sea level rise at the top, deep progressive facies, extremely reducing conditions, elevated organic production, and euxinic conditions.
	EBc_{17}	4557	OSF2	7.85	2.47	5.34	17.46	1.7×10^{-3}	4.6×10^{-3}	0.14	3.6	0.44	8.02	137.66	17.16	29.93	
	EBc_{18}	4566	OSF1	3.62	2.12	2.61	11.94	5.2×10^{-3}	1×10^{-2}	0.14	3.09	0.4	22.19	245.52	11.06	37.84	Progressive facies, warm to hot waters from the shelf environment, high salinity, closed sedimentary basin, anoxic to suboxic conditions.
Balad	Bac_1	3959	OSF3	1.22	0.42	0.76	7.0	1.65×10^{-3}	4.1×10^{-3}	0.19	9.76	0.075	7.63	146.34	19.17	73.77	Regressive facies, suboxic to dysoxic conditions.
	Bac_2	3977	OSF3	1.57	0.55	0.77	6.15	7.6×10^{-4}	1.7×10^{-3}	0.09	10.02	0.088	2.28	28.98	12.71	25.47	
	Bac_3	3990	OSF3	1.27	– 0.3	0.79	9.54	9.1×10^{-4}	3.8×10^{-3}	0.12	13.52	0.13	4.51	76.36	16.93	49.6	
	Bac_4	4001	OSF1	2.31	1.28	1.52	8.75	2.1×10^{-3}	5.5×10^{-3}	0.21	10.07	0.1	11.39	152.11	13.35	49.78	Regressive facies, anoxic to suboxic conditions.
	Bac_5	4004	OSF5	1.9	0.7	1.41	8.78	1.7×10^{-3}	3.8×10^{-3}	0.1	6.5	0.08	6.67	189.65	28.43	57.89	Progressive facies, suboxic conditions.
	Bac_6	4007	OSF5	2.18	0.99	1.36	7.93	1.9×10^{-3}	3.6×10^{-3}	0.9	6.55	0.09	6.79	123.84	18.23	55.04	
	Bac_7	4009	OSF5	2.7	1.25	1.5	9.11	2.1×10^{-3}	4.5×10^{-3}	0.15	6.4	0.11	7.57	201.51	26.61	49.26	
	Bac_8	4015	OSF1	3.90	1.10	1.62	9.31	1.4×10^{-3}	5.3×10^{-3}	0.14	11.52	0.11	8.4	127.27	15.15	32.3	Regressive facies, tropical climate, low organic production, anoxic to suboxic conditions.
	Bac_9	4025	OSF2	4.42	2.0	2.97	17.14	1.5×10^{-3}	5.8×10^{-3}	0.14	12.0	0.1	7.88	167	21.19	46.83	Sea level rise at the top, deep progressive facies, extreme reducing conditions, elevated organic production, and euxinic conditions.
	Bac_{10}	4037	OSF3	0.39	– 0.07	0.77	9.0	9.4×10^{-4}	3.5×10^{-3}	0.1	8.37	0.1	5.37	114.62	21.34	251.28	Regressive facies, increased organic production, suboxic to dysoxic conditions.
	Bac_{11}	4058	OSF3	1.12	0.35	0.97	9.58	1.0×10^{-3}	3.2×10^{-3}	0.08	7.23	0.16	3.89	61.55	15.82	58.03	
	Bac_{12}	4077	OSF3	1.24	0.79	1.15	9.76	1.0×10^{-3}	4.4×10^{-3}	0.11	4.5	0.15	5.82	59.02	10.14	41.13	
	Bac_{13}	4087	OSF2	4.11	2.15	4.5	17.92	1.7×10^{-3}	6.3×10^{-3}	0.14	4.06	0.33	9.85	157.99	16.03	42.09	Sea level rise at the top, deep progressive facies, extreme reducing conditions, elevated organic production, and euxinic conditions.
	Bac_{14}	4094	OSF1	3.15	0.44	1.92	10.31	2×10^{-3}	6.2×10^{-3}	0.17	5.13	0.36	11.18	184.34	16.48	46.35	Progressive facies, warm to hot waters from the shelf environment, high salinity, closed sedimentary basin, anoxic to suboxic conditions.

Results

Organic Sedimentary Facies One (OSF.1)

As shown in Figures 3 and 4, as well as Tables 1 and 2, OSF1, observed at depths of 4566–4570, 4532–4545, and 4465–4471 m in EB1 and 4091–4095, 4009–4017, and 3994–4004 m in Ba1, has relatively high TOC contents, with averages of 4.36 % for EB1 and 3.12 % for Ba1. The TOC ranges from 3.55 to 5.75 wt.% in EB1 and 2.31 to 3.9 wt.% in Ba1, showing a decreasing trend from bottom to top (Fig. 3). There is a notable fluctuation range in the $\delta^{98/95}$Mo values, ranging from 1.51 ‰ to 2.12 ‰ in EB1 and from 0.44 ‰ to 1.32 ‰ in Ba1. For EB1 and Ba1, the U/Th ratios are 2.42–2.61 and 1.52–1.92, and the Ni/Co ratios are 9.21–11.94 and 8.75–10.31, respectively, (Fig. 3). The enrichment factors for EF(U) (11.13–22.19 for EB1 and 8.4–11.39 for Ba1), and EF(Mo) values (128.96 –254.9 for EB1 and 127.27–184.34 for Ba1), showing comparatively high values and similar variations (Fig. 4). Additionally, EB1 and Ba1 have relatively high Ni/Al ratios, ranging from 5.9 × 10^{-3} to 1 × 10^{-2} for EB1 and 5.3 × 10^{-3} to 6.2 × 10^{-3} for Ba1, and Cu/Al ratios ranging from 2.4 × 10^{-3} to 5.2 × 10^{-3} for EB1, and 1.4 × 10^{-3} to 2.1 × 10^{-3} for Eb1, respectively (Fig. 3).

Organic Sedimentary Facies Two (OSF.2)

OSF.2 was observed at depths of 4545– 4566 and 4471– 4481 m in EB1, and 4078 – 4091 and 4017–4026 m in Ba1. The TOC content ranges from 6.74 to 8.0 wt.% in EB1, and from 4.11 to 4.42 wt.% in Ba1, with averages of 7.61 % and 4.26 %, respectively (Table 1 & 2). The $\delta^{98/95}$Mo values for EB1 and Ba1 range from 2.09 ‰ to 2.5 ‰ and from 2.0 ‰ to 2.15 ‰, respectively, and progressively increase from the bottom to the centre of the facies (4472 m for EB1 and 4025 m for Ba1) before declining. Compared to OSF1, the U/Th ratios (3.53–5.59 for EB1 and 2.97–4.5 for Ba1) and Ni/Co ratios (10.3–17.46 for EB1 and 17.14–17.92 for Ba1) (Fig. 3), and the enrichment factors of EF(U) (8.02–15.95 for EB1 and 7.88–9.85 for Ba1) and EF(Mo) values (137.66–287.39 for EB1 and 157.99–167 for Ba1), show compara-

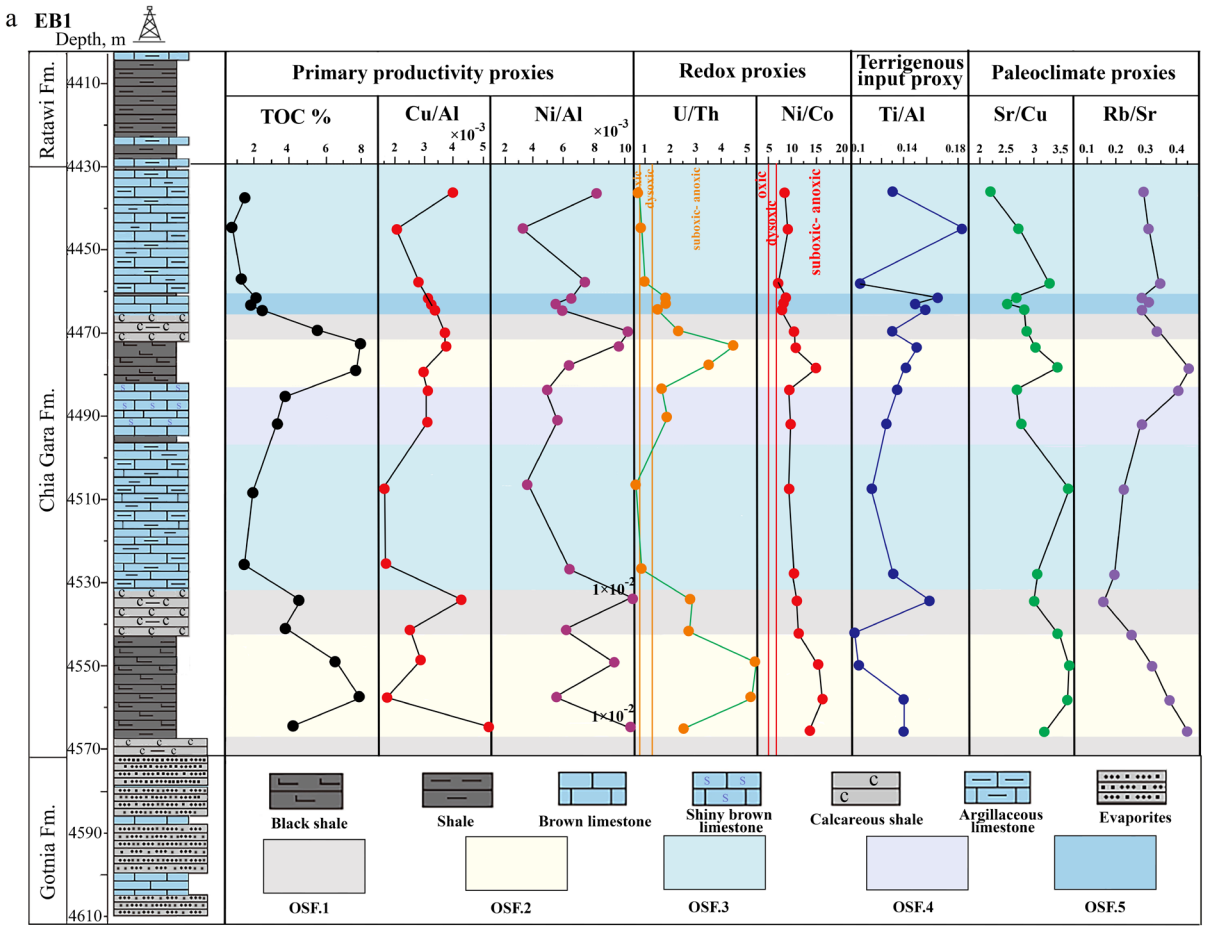

Fig. 3. Vertical changes in the amounts of total organic carbon (TOC), primary productivity proxies (Cu/Al, Ni/Al), redox proxies (U/Th, Ni/Co), and terrigenous input proxies (Ti/Al), in (a) East Baghdad Oilfield and (b) Balad Oilfield.

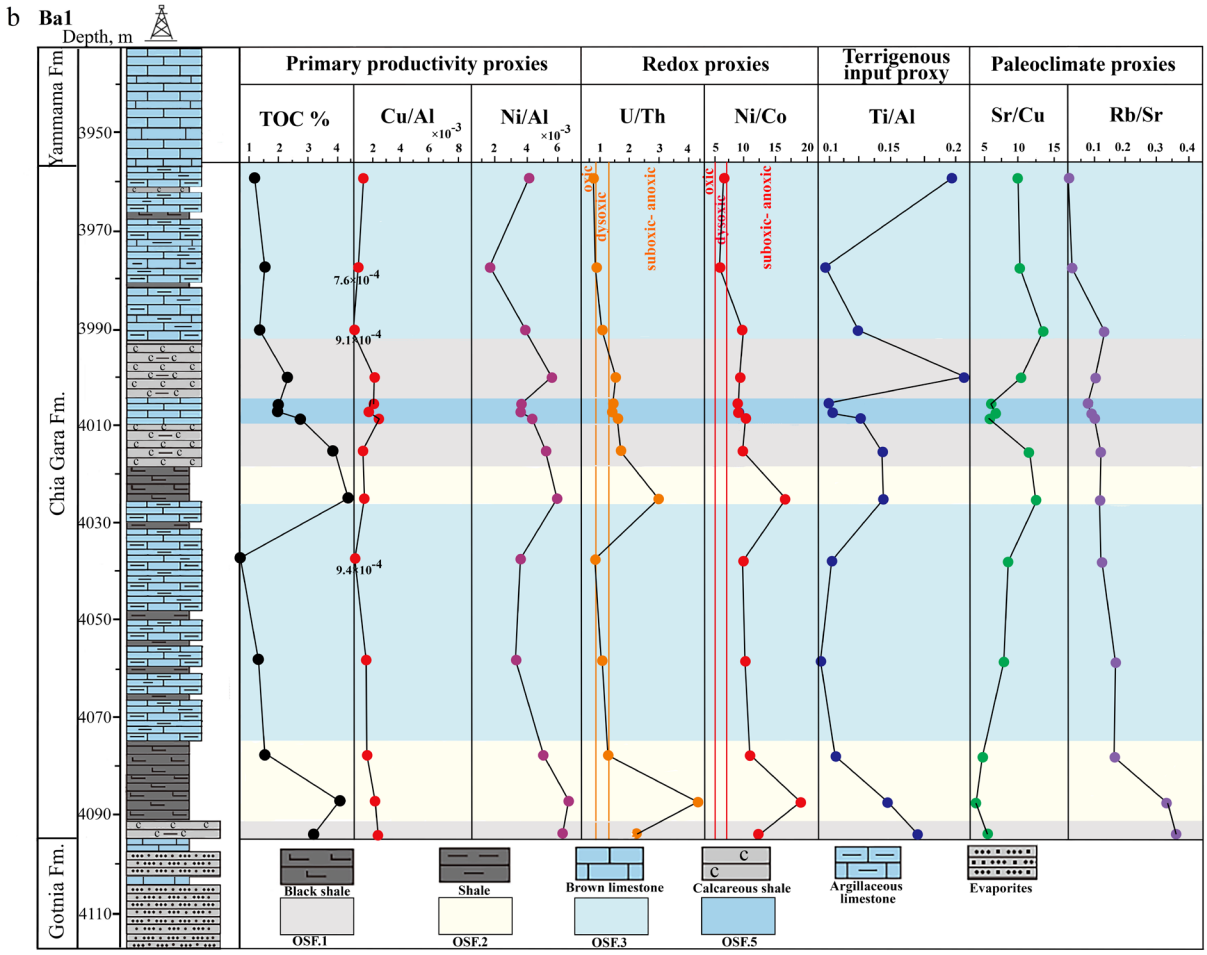

Fig. 3. Vertical changes in the amounts of total organic carbon (TOC), primary productivity proxies (Cu/Al, Ni/Al), redox proxies (U/Th, Ni/Co), and terrigenous input proxies (Ti/Al), in (a) East Baghdad Oilfield and (b) Balad Oilfield.

tively stable values (Fig. 4; Table 1). For EB1 and Ba1, the Ni/Al ratios range from 4.6 × 10^{-3} to 9.5 × 10^{-3} and from 5.8 × 10^{-3} to 6.3 × 10^{-3}, respectively, while the Cu/Al ratios range from 1.7 × 10^{-3} to 3.9 × 10^{-3} and from 1.5 × 10^{-3} to 1.7 × 10^{-3}. These ratios show similar patterns (Fig. 3; Table 2), with higher values at the bottom and lower values at the top part of OSF2.

Organic Sedimentary Facies Three (OSF.3)

In OSF.3, observed at depths of 4494– 4532 m and 4430– 4461 m in EB1, and 4026– 4078 m and 3958– 3994 m in Ba1, the TOC content ranges from 0.5 to 1.9 wt.% and 0.39 to 1.57 wt.%, with averages of 1.56 % and 1.13 % for EB1 and Ba1, respectively (Tables 1 & 2). These values are comparatively lower than those of OSF1 and OSF2, and they progressively decline upwards. For EB1 and Ba1, the $\delta^{98/95}$Mo values remain relatively stable ranging from – 0.25 ‰ to – 0.61 ‰ and – 0.35 ‰ to – 0.79 ‰, respectively, with a downward trend vertically (Fig. 4). The U/Th ratios (0.76–0.88 for EB1 and 0.76–1.15 for Ba1) and Ni/Co ratios are (6.15–7.75 for EB1 and 6.15–9.76 for Ba1) (Fig. 3), as well as the enrichment factors of EF(U) (4.0–10.43 for EB1 and 2.28–7.63 for Ba1) and EF(Mo) values (36.84–108.88 for EB1 28.98–146.34 for Ba1) for EB1 and Ba1, are all relatively low and show minor fluctuations (Fig. 4; Table 3). Compared to OSF1 and OSF2, the Ni/Al ratios (3.4 × 10^{-3} to 8.1 × 10^{-3} for EB1 and 1.7 × 10^{-3} to 4.4 × 10^{-3} for Ba1) and Cu/Al ratios (1.4 × 10^{-3} to 4.0 × 10^{-3} for EB1 and 7.6 × 10^{-4} to 1.65 × 10^{-3} for Ba1) decrease progressively from the bottom of the interval and then increase towards the top (Fig. 3; Table 3).

Organic Sedimentary Facies Four (OSF.4)

In OSF.4, observed at depths of 4481–4494 m in EB1, the TOC content ranges from 2.95 to 3.77 wt.%, with an average of 3.36 % for EB1. This value is higher than that of OSF3 but lower than those of OSF1 and OSF2 (Table 1 & 2). The EB1 $\delta^{98/95}$Mo values decreased further, from 1.39 ‰

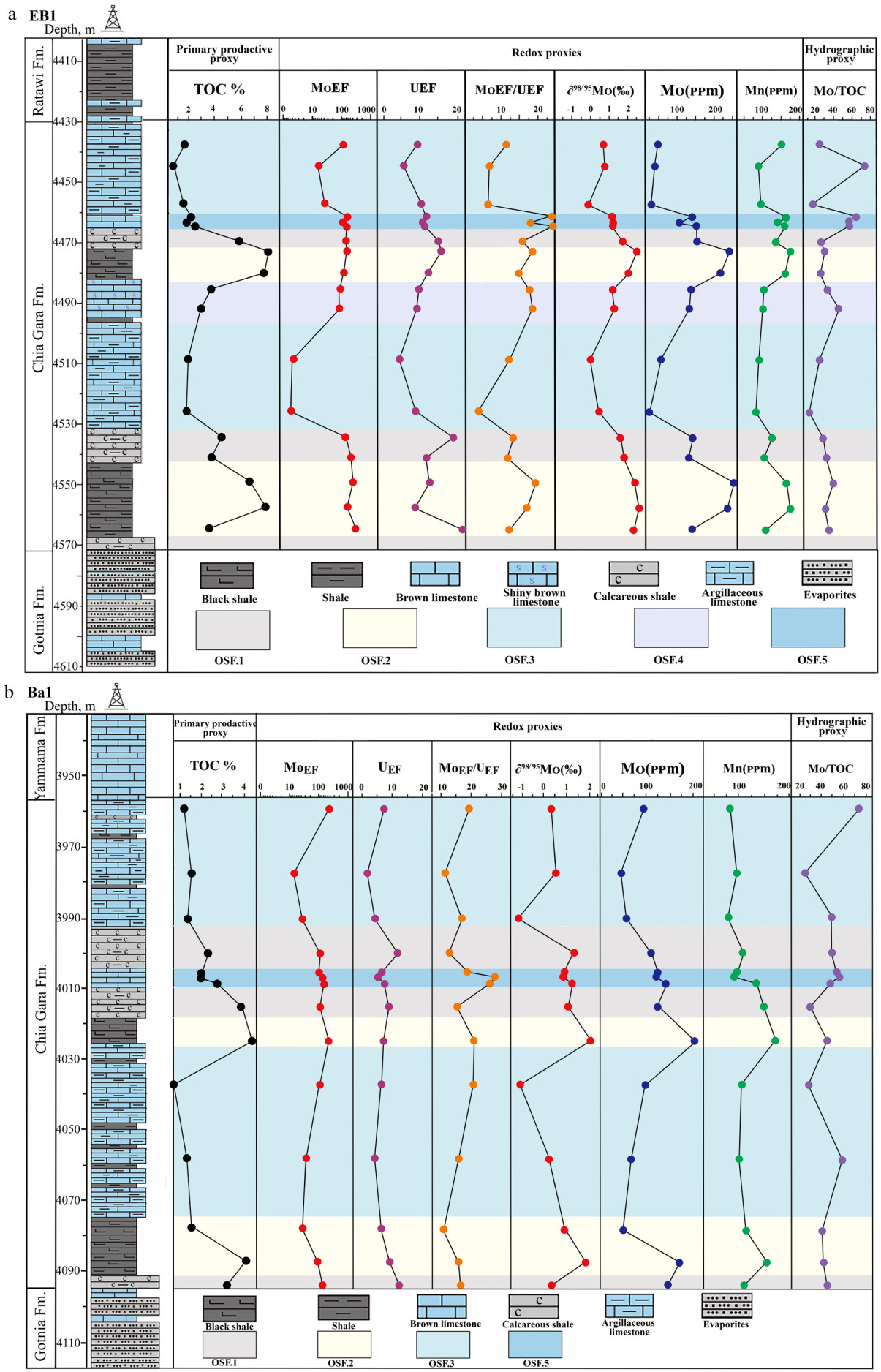

Fig. 4. Primary productivity proxy (TOC %), hydrographic proxy (Mo/TOC) and redox proxies (MoEF, UEF, MoEF/UEF, $\delta^{98/95}$Mo, Mo, and Mn) with vertical variations, (a) in the East Baghdad Oilfield and (b) in the Balad Oilfield.

Table 3. Tithonian–Berriasian Chia Gara Formation with $\delta^{98/95}$Mo values.

Oilfield	Samples	Depth (m)	Organic sedimentary facies (OSF)	$\delta^{98/95}$Mo (‰)	$\delta^{98/95}$Mo (auth.)[2] (‰)	$2\sigma x^2$
East Baghdad	EBc_1	4437	OSF3	0.59	0.59	0.02
	EBc_2	4445	OSF3	0.61	0.64	0.03
	EBc_3	4457	OSF3	– 0.1	– 0.1	0.02
	EBc_4	4461	OSF5	1.11	1.12	0.02
	EBc_5	4464	OSF5	1.17	1.19	0.04
	EBc_6	4465	OSF5	1.09	1.11	0.04
	EBc_7	4470	OSF1	1.59	1.62	0.03
	EBc_8	4472	OSF2	2.5	2.54	0.02
	EBc_9	4480	OSF2	2.09	2.1	0.03
	EBc_{10}	4485	OSF4	1.07	1.07	0.03
	EBc_{11}	4493	OSF4	1.15	1.15	0.02
	EBc_{12}	4509	OSF3	– 0.25	– 0.26	0.03
	EBc_{13}	4527	OSF3	0.54	0.53	0.03
	EBc_{14}	4533	OSF1	1.51	1.55	0.03
	EBc_{15}	4541	OSF1	1.67	1.68	0.02
	EBc_{16}	4549	OSF2	2.33	2.30	0.02
	EBc_{17}	4557	OSF2	2.47	2.48	0.04
	EBc_{18}	4566	OSF1	2.12	2.16	0.03
Balad	Bac_1	3959	OSF3	0.42	0.45	0.02
	Bac_2	3977	OSF3	0.55	0.58	0.04
	Bac_3	3990	OSF3	– 0.3	– 0.35	0.02
	Bac_4	4001	OSF1	1.28	1.32	0.03
	Bac_5	4004	OSF5	0.7	0.9	0.03
	Bac_6	4007	OSF5	0.99	1.04	0.03
	Bac_7	4009	OSF5	1.25	1.21	0.03
	Bac_8	4015	OSF1	1.10	1.13	0.02
	Bac_9	4025	OSF2	2.0	2.07	0.02
	Bac_{10}	4037	OSF3	– 0.07	– 0.14	0.03
	Bac_{11}	4058	OSF3	0.35	0.33	0.04
	Bac_{12}	4077	OSF3	0.79	0.8	0.02
	Bac_{13}	4087	OSF2	2.15	2.37	0.02
	Bac_{14}	4094	OSF1	0.44	0.44	0.03

to 1.00 ‰ (Fig. 4). Within this interval, the U/Th ratio ranges from 1.64 to 1.88, and the Ni/Co ratio ranges from 7.26 to 7.35 ratios (Fig. 3). The EF(U) ranges from 9.2 to 9.6, and EF(Mo) from 169.21 to 169.29 for EB1, indicating comparatively low enrichment degrees (Fig. 4; Table 3). The Ni/Al ratio varies from 5.2×10^{-3} to 5.7×10^{-3}, and Cu/Al ratio 2.9×10^{-3} to 3.0×10^{-3}, both increasing noticeably compared to the OSF3 and showing a progressive upward trend (Fig. 3; Table 3).

Organic Sedimentary Facies Five (OSF.5)

In OSF.5, observed at depths of 4461–4465 m in EB1, and 4004–4009 m in Ba1, the TOC content ranges from 1.9 to 2.5 wt.%, and 1.9 to 2.7 wt.%, with averages of 2.2 % and 2.26 %, for wells EB1 and Ba1, respectively (Table 1 & 2). This is lower than the TOC content of all other facies except OSF3. EB1 and Ba1 have rather stable $\delta^{98/95}$Mo values, with a decreasing trend upwards and ranges of 1.09 ‰ to 1.17 ‰ and 0.7 ‰ to 1.25 ‰, respectively (Fig.4). The U/Th ratios (1.54–1.84 for EB1 and 1.36–1.5 for Ba1) and Ni/Co ratios (6.5–

7.94 for EB1 and 7.93–9.11 for Ba1) (Fig. 3; Table 3), as well as the enrichment factors for the EF(U) values (10.45–11.4 for EB1 and 6.67–7.57 for Ba1) and EF(Mo) values (185.69–286.03 for EB1 and 123.84–201.51 for Ba1) indicate relatively low degrees of enrichment (Fig. 4; Table 3). In contrast to the other facies, the Ni/Al ratios (5.57×10^{-3} to 6.08×10^{-3} for EB1 and 3.6×10^{-3} to 4.5×10^{-3} for Ba1) and Cu/Al ratios (3.1×10^{-3} to 3.3×10^{-3} for EB1 and 1.7×10^{-3} to 2.1×10^{-3} for Ba1) increased significantly.

Discussion

Evaluations the degree of oxygenation in the bottom water environment

Paleoceanic redox conditions have been extensively reconstructed using U/Th and Ni/Co ratios (Algeo et al., 2020; Abshire et al., 2021; Al-Khatony et al., 2023; Chen et al, 2023; Zhang et al., 2023). Anoxic conditions are indicated by U/Th >1.25 and Ni/Co > 7; dysoxic conditions are inferred from 0.75 < U/Th < 1.25 and 5 < Ni/Co < 7; and oxic conditions are implied by U/Th < 0.75 and Ni/Co < 5 (Jones & Manning, 1994). Anoxic-suboxic environments are reflected in the relatively high U/Th ratios (averages of 2.52 and 1.68) and Ni/Co ratios (averages of 10.91 and 9.45) for EB1 and Ba1, respectively, in OSF1. In OSF4, the U/Th ratio (average 1.76) and Ni/Co ratio (average 7.30) for EB1, and in OSF5, the U/Th ratio (average 1.72) and the Ni/Co ratio (average 7.26) for EB1, and the U/Th ratio (average 1.42) and the Ni/Co ratio (average 8.60) for Ba1, respectively (Table 1), also indicate similar conditions. A reasonably stable euxinic environment is reflected in the comparatively higher values of these ratios in OSF2: U/Th (average 4.74) and Ni/Co (average 14.29) for EB1 and U/Th (average 3.73) and Ni/Co (average 17.53) for Ba1, respectively (Table 2). A comparatively steady oxic-dysoxic environment is indicated by the relatively low values of these ratios in OSF3: U/Th (average 0.82) and Ni/Co (average 7.23) for EB1 and U/Th (average 0.86) and Ni/Co (average 8.5) for Ba1, respectively (Fig.3). An upward trend in the oxidation condition of the bottom water column in the Mesopotamian Fore Deep Basin is indicated by relatively low U/Th and Ni/Co ratios (Fig.3). The redox conditions deduced from EF(Mo)/EF(U), Mo/TOC ratios, and Mo content (Figs. 4 & 5a) are consistent with this interpretation.

Note that the absence of open ocean inputs in restricted regions may result in a decrease in Mo levels in the water columns (Algeo et al., 2008). The anoxic-suboxic environment in OSF1 is supported by the U/Th and Ni/Co ratios, which indicate an average Mo content of 141.25 mg/kg and 129 mg/kg and an average EF(Mo)/EF(U) ratio of 12.93 and 14.99 for EB1 and Ba1, respectively. Two cycles of increasing and decreasing OSF2 can be identified by combining the sea-level change curve with redox-sensitive trace-element proxies, including U, Mo, and their enrichment factors (EF(U) and EF(Mo)) (Figs. 2 & 4).

Two transgressive events correspond to the respective high points of these cycles (EBc_{15} at 4541 m and EBc_7 at 4470 m for EB1 and Bac_{12} at 4077 m and Bac_8 at 4015 m for Ba1). The extensive incursions increased the degree of water reduction and replenished trace elements (U, Mo, etc.) by connecting the Fore Deep Basin to the open sea. The TOC and ratios of redox-sensitive trace elements such as U/Th, Cu/Al, and Ni/Al do not show significant correlation at these points (Ritzer et al., 2024) (Fig. 6a-f), suggesting that euxinic conditions may have occurred at 4545 m and 4471 m in EB1 and 4078 m and 4017 m in Ba1 (Fig. 4).

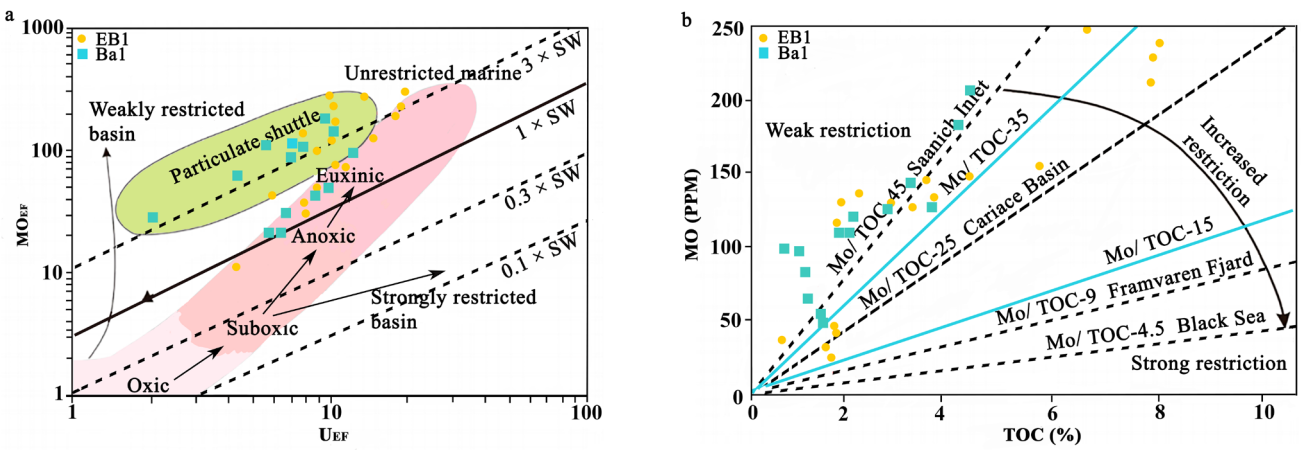

Fig. 5. (a) U_{EF} vs Mo_{EF} for Chia Gara Formation samples (Algeo et al., 2009; Tribovillard et al., 2012). The solid line indicates the Mo/U ratio of modern seawater. (b) Sediment Mo vs TOC for samples from the Chia Gara Formation.

Given the anoxic-suboxic conditions suggested by the U/Th and Ni/Co ratios in OSF1, OSF4, and OSF5, the EF(Mo)/EF(U) ratios (averages of 12.93, 18.01, and 22.69 for EB1), and in OSF1 and OSF5, the EF(Mo)/EF(U) ratios (averages of 14.99 and 24.42 for Ba1) most likely indicate prevailing anoxic-suboxic water conditions with sporadic and slightly euxinic conditions. In the OSF1 and OSF3 facies, low-oxidising bottom water conditions developed concurrently with the Tithonian–Berriasian regression event. Low EF(Mo)/EF(U) ratios (averages of 12.93 and 8.43 for EB1, and 14.99 and 16.01 for Ba1), which indicate a suboxic-dysoxic environment, are consistent with this interpretation. The Chia Gara Formation's bottom water environment was, from bottom to top, anoxic-suboxic, euxinic, anoxic-suboxic, dysoxic, suboxic, euxinic, anoxic-suboxic, suboxic, dysoxic for EB1 and anoxic-suboxic, euxinic, suboxic-dysoxic, euxinic, anoxic-suboxic, suboxic, anoxic-suboxic, suboxic, anoxic-suboxic, suboxic-dysoxic for Ba1 (Fig. 5a). The basin's hydrographic conditions directly affect the redox conditions in the bottom water. A common indicator of basin water connection constraints is the Mo/TOC ratio (Wang et al., 2024) (Fig. 5b). However, because Upper Jurassic–Early Cretaceous oceans may have had higher Mo content than modern seawater (Pearce et al., 2010; Hovikoski et al., 2023, Cheng et al., 2016) proposed that good connectivity between the basin and the open sea may be inferred when the Mo/TOC ratio in sediments exceeds 11 mg/kg/wt.%. The comparatively high Mo/TOC ratios in OSF1 (averages of 33.26 and 42.81 mg/kg /wt.% for EB1 and Ba1, respectively) reflect low basin water restriction, which is conducive to the presence of anoxic-suboxic bottom water environments. The two transgression events are well-matched by the Mo/TOC values in OSF2, showing that basin openness increases during transgressions. The regression during the Tithonian–Berriasian transition is reflected in the suboxic-dysoxic environment in OSF3 (Figs. 2 & 4). Additionally, reduced connectivity between the basin and the open sea restricts the replenishment of dissolved Mo in the water column, leading to lower U and Mo values (averages of 9.30 and 37 for EB1, and 8.71 and 67.83 for Ba1, respectively). Although lower than the OSF2 values, the Mo/TOC levels in OSF4 (EB1) closely correspond to the transgression event. Mo/TOC levels increased further with a continued decline in basin restrictiveness in OSF5 (Fig. 5b).

The redox conditions associated with $\delta^{98/95}$Mo

Since Mo isotopes are highly sensitive to redox conditions, they have been routinely employed in organic-rich sedimentary rocks to reconstruct local and global marine redox states (Lu et al., 2020; Nan et al., 2023). The ocean produces Mo primarily in two ways. The light Mo isotope is preferentially adsorbed by manganese or iron oxides under oxic conditions, leading to up to 3 % isotope fractionation between sediments and seawater (Jia et al., 2023). At high H_2S concentrations ([H_2S]aq > 11 μM) in euxinic settings, the primary form of Mo in modern seawater, the oxyanion molybdate (MoO_4^{2-}), is almost entirely transformed into the oxythiomolybdate molecule ($MoO_{4-x}S_x^{2-}$, x=1–4), with minimal isotope fractionation (Vorlicek et al., 2018). At low H_2S concentrations ([H_2S]aq < 11μM) in aqueous solutions, molybdate (MoO_4^{2-}) conversion is insufficient, resulting in considerable isotope fractionation in sedimentary Mo isotopes (Nan et al., 2023). This also explains the ability of Mo isotopes to function as redox proxies. Using the approach suggested by Tsujisaka et al. (2019), we removed any potential detrital effects by leaching with 4 M or more concentrated HCl after ashing, prior to analysing the Mo isotopes. The adjusted findings demonstrate that there is little effect of detrital Mo on bulk Mo isotopes, with the measured Mo isotope levels ($\delta^{98/95}$Mo) being almost equal to the correct values ($\delta^{98/95}Mo_{auth}$) (Table 1). The presence of euxinia in anoxic bottom water environments has been confirmed by $\delta^{98/95}$Mo readings from the deep outer shelf's EB1 and Ba1 cores. At the OSF3, negative $\delta^{98/95}$Mo values (– 0.1 to – 0.25 ‰ in EB1 and – 0.07 to – 0.3 ‰ in Ba1) are observed (Fig. 4). Three potential mechanisms are often responsible for the presence of negative Mo isotopes. The lower U/Th and Ni/Co ratios in OSF3 support the first hypothesis, which is Fe-Mn_{ox} adsorption in the oxic environment (Okuyama et al., 2025).

The second hypothesis is Fe-Mn_{ox} shuttling, which is comparable to processes observed in the Baltic Sea and the Cariaco Basin today (Lenstra et al., 2020). The shuttling action of iron and manganese oxides causes lighter Mo isotopes (lighter $^{98/95}$Mo) to enter the sediments, resulting in negative $\delta^{98/95}$Mo values. In this context, the sediment's euxinic conditions favour the enrichment of Mo over U, leading to higher EF(Mo)/EF(U) ratios (~3 × SW) and comparatively greater Mo contents.

However, the absence of reductive dissolution prevents Mn from accumulating in the sediment,

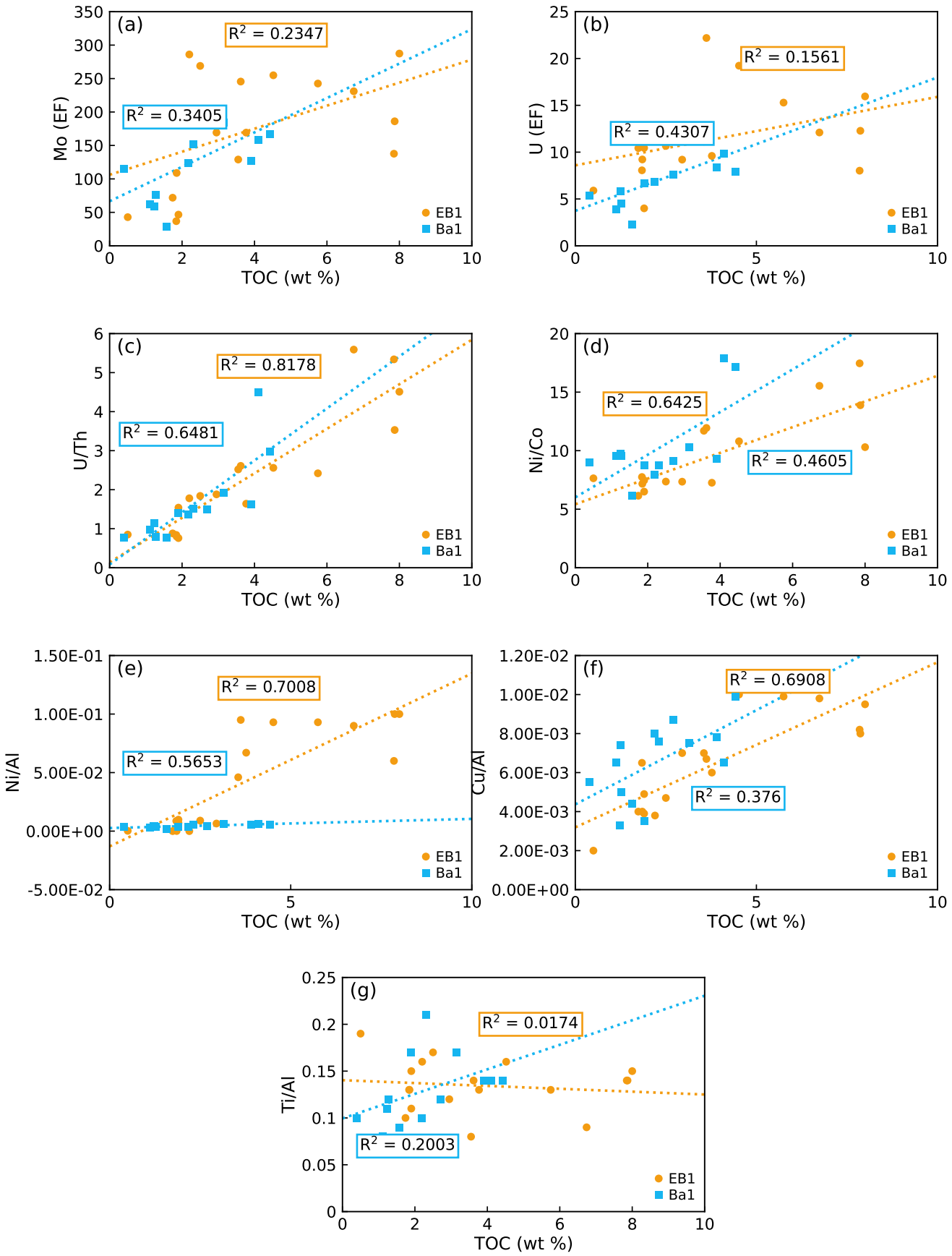

Fig. 6. Correlations between TOC contents and the following ratios in Chia Gara Formation samples: (a) Mo (EF); (b) U (EF); (c) U/Th; (d) Ni/Co; (e) Ni/Al, $P(\alpha) < 0.05$; (f) Cu/Al, $P(\alpha) < 0.05$; and (g) Ti/Al.

leading to a relative Mn shortage. Fe-Mn_{ox} shuttling is supported by the EF(Mo)/EF(U) ratios (6.89 and 21.34), Mo (33 and 98 mg/kg), and Mn (100 and 105 mg/kg) values in samples EBc_3 and Bac_{10}, respectively, near the bottom of OSF3. It is important to note that samples EBc_{12} and Bac_3 also support the hypothesis of Fe-Mn_{ox} shuttling due to their negative $\delta^{98/95}$Mo values (– 0.3 ‰ and –0.25 ‰, respectively). The third theory is based on the incomplete conversion of molybdate (MoO_4^{2-}) in euxinic water ([H_2S]aq < 11 μM), which results in Mo isotope fractionation (Nagler et al., 2011). The potential for Fe-Mn_{ox} shuttling is excluded because samples with negative $\delta^{98/95}$Mo values in OSF3 have EF(Mo)/EF(U) ratios only about twice those of contemporary seawater (~1 × SW). Consequently, the substantial fractionation caused by the partial conversion of molybdate (MoO_4^{2-}) in euxinic waters may also be the origin of the low $\delta^{98/95}$Mo values in OSF3.

The $\delta^{98/95}$Mo values of samples EBc_8 (2.5 ‰) and EBc_{17} (2.47 ‰) in OSF2 are comparatively high, except for the negative values. The highest $\delta^{98/95}$Mo values of Late Jurassic oceanic seawater may be represented by the values reported by Pearce et al. (2010) (~ + 2.46 ‰). These two high values are almost equal to immediate seawater $\delta^{98/95}$Mo values (Fig. 4), which may indicate lower isotope fractionation under high H2S conditions. The $\delta^{98/95}$Mo values fluctuate in OSF3 and the lower part of OSF2 (prior to the transgression) (–0.25 to 0.61 in EB1 and –0.3 to 0.79 in Ba1; Fig. 3). Except for the previously described samples EBc_3, Bac_{10}, EBc_{12}, and Bac_3, none of the other samples showed Fe-Mn_{ox} shuttling. Such a wide range of fluctuations may represent isotope fractionation in euxinic water (Nagler et al., 2011; Gomes et al., 2015). Ultimately, the emergence of euxinic conditions in the intra-shelf basin is suggested by the overall oscillations in OSF1 and 2, as well as by the extreme points that are partially evident. The $\delta^{98/95}$Mo isotopic composition of molybdenum shows a declining trend, demonstrating a negative bias from the incursion of the Late Jurassic-Early Cretaceous, from 4470 m in OSF1 to 4430 m in OSF3 of EB1 and from 4015 m in OSF1 to 3955 m in OSF3 of Ba1 (Figs. 2 & 4). The $\delta^{98/95}$Mo in the intra-shelf seawater may then gradually decline to

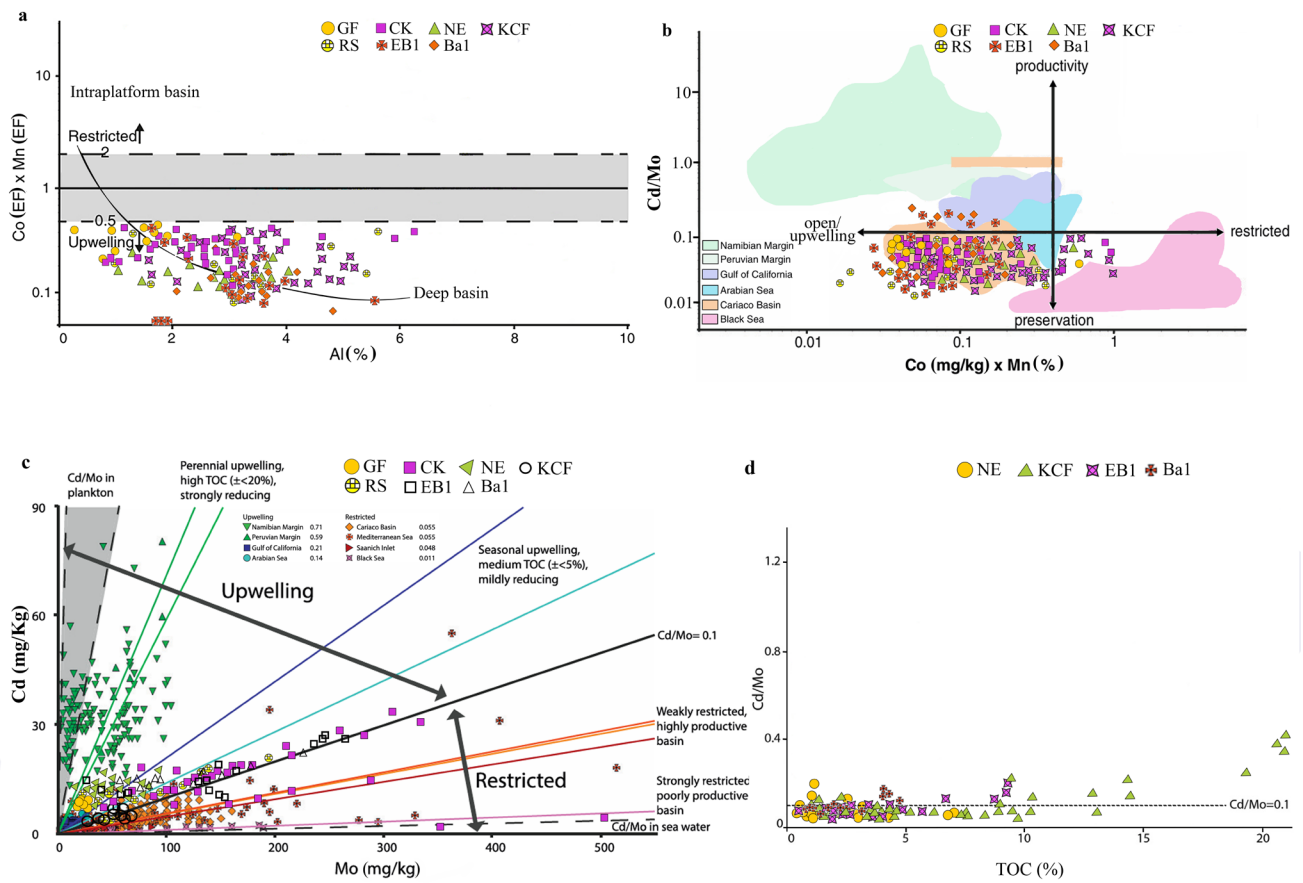

Fig. 7. Cross-plots of (a) Al versus Co(EF)× Mn(EF), (b) Co (mg/kg) × Mn (%) versus Cd/Mo ratios, (c) Mo (mg/Kg) versus Cd (mg/kg), and (d) TOC (%) versus Cd/Mo ratios for the Chia Gara Formation and its equivalent samples (Sweere et al., 2016). The published data from various sections and wells in the Cretaceous and Upper Jurassic are the sources of the sample data in a, b, c, and d. Information from: GF (Al-Bayati, 1998); CK (Mustafa et al., 2020); NE (Mohialdeen & Raza, 2013); KCF (Al-Ameri, 2011); RS (Al-Khatony et al., 2023); EB1 and Ba1: this study.

levels close to those of continental input as a result of continuous regression, which increased the confinement of the intra-shelf basin (+0.59 and +0.42 for EB1 and Ba1, respectively) (Fig. 4).

Primary productivity

Prior research has indicated that several geochemical markers, such as TOC values, organic biomarkers, N and C isotopes, and additional trace elements including Ba, Cu, Ni, and P, can be used to reconstruct primary productivity (Shi et al., 2022). Organic matter (OM) in sediments is often associated with Ni and Cu, which are essential nutrients for phytoplankton growth in the photic zone (Tribovillard et al., 2006). As a single measure may not provide an adequate estimate of primary productivity (Schoepfer et al., 2015), we examined differences in primary productivity using multiple indicators (TOC, Ni, and Cu) and accounted for the dilutive effect of detrital components on Ni and Cu. Minor uncertainties in the choice of detrital Ni/Al and Cu/Al ratios do not affect calculated Ni_{org} and Cu_{org} fluxes, as detrital Ni and Cu constituted less than 5 % of total Ni and Cu in all study facies. In most open-ocean environments, the estimated proportions of detrital Ni and Cu are so small as to be practically negligible.

The results indicated that most Ni and Cu are associated with OM and may be used to reconstruct primary productivity in surface waters. The Ni/Al and Cu/Al ratios showed a strong to moderate correlation with TOC (Fig. 6e, f) (R^2= 0.7 for EB1 and 0.57 for Ba1, P(α) < 0.05 for Ni/Al vs. TOC and R^2=0.69 for EB1 and 0.37 for Ba1 (weak correlation), P(α) < 0.05 for Cu/Al vs. TOC) (Tribovillard et al., 2006). In the Chia Gara Formation, the shale Ni/Al ratios decreased slightly from OSF1 ($5.9 \times 10^{-3} - 1 \times 10^{-2}$, average 8.95×10^{-3}) to OSF4 ($5.2 \times 10^{-3} - 5.7 \times 10^{-3}$, average 5.45×10^{-3}) and then increased in OSF2 ($4.6 \times 10^{-3} - 9.5 \times 10^{-3}$, average 7.42×10^{-3}) in EB1, while in Ba1 they decreased from OSF1 ($5.3 \times 10^{-3} - 6.2 \times 10^{-3}$, average 5.66×10^{-3}) to OSF3 ($1.7 \times 10^{-3} - 4.4 \times 10^{-3}$, average 3.45×10^{-3}) and then increased in OSF2 ($5.8 \times 10^{-3} - 6.3 \times 10^{-3}$, average 6.05×10^{-3}), indicating a modest decrease in surface water bioproductivity, followed by a notable increase (Fig. 3). Additionally, a similar pattern was observed in the TOC values and Cu/Al ratios.

This result aligns with previous research findings that the well-developed upwelling occurrences in deep-water slope and basinal facies are more productive than those in intraplatform basin facies. Upwelling events, frequently documented in various Jurassic-Upper Cretaceous facies, are

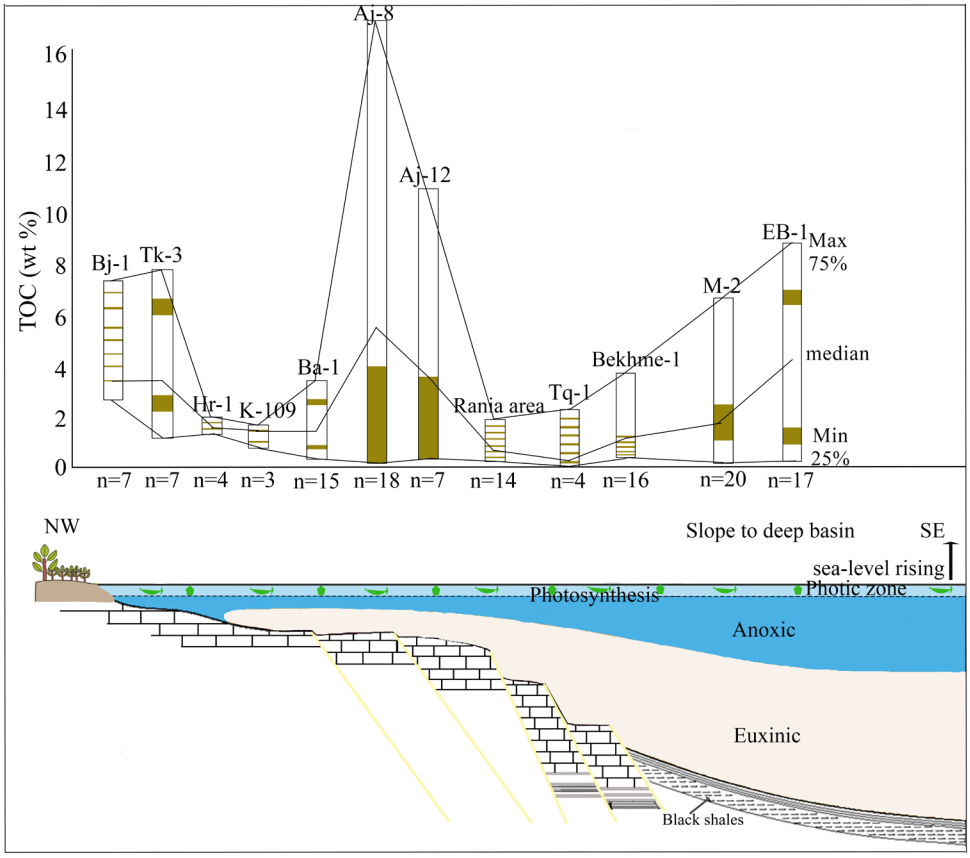

Fig. 8. A simplified model for the factors controlling organic matter accumulation during shale deposition of Chia Gara Formation in central and northern Iraqi facies regions. The following sources provide TOC data for wells and sections: Mohialdeen & Hakimi (2016), Al-Beyati et al. (2021), Al-Khatony et al. (2023), Al-Ameri et al. (2012b), Al-Ahmed (2013), and Al-Ameri (2011), Ali (2018), Damoulianou et al. (2022).

one of the key factors influencing OM accumulation (Figs. 7a, b & 8). Since upwelling from the sea bottom is often enriched in Cd and somewhat depleted in Co and Mn, upwelling is considered present when EF(co) × EF(Mn) < 0.5 or Co × Mn < 0.4. In contrast, a restricted environment is indicated when EF(Co) × EF(Mn) > 2 or Co × Mn > 0.4 (Sweere et al., 2016) (Fig. 7a). As shown in Figures 7a and b, the Chia Gara Formation's EF(Co) × EF(Mn) values (0.05–0.48, average 0.19 for EB1 and 0.05–0.33, average 0.14 for Ba1) and Co × Mn values (0.04–0.27, average 0.18 for EB1 and 0.03–0.22, average 0.11 for Ba1) suggest a relatively upwelling environment, further corroborated by the comparatively low Mo and Cd/Mo ratios (Figs. 7c & d). Profiles of EF(co)× EF(Mn), Co × Mn, and Mo values within different sedimentary facies reveal a progressive increase in upwelling events from the deep-water slope to the basinal facies (Figs. 7a, b & c). Alongside this trend, TOC values gradually increase (Fig. 7d & 8). Upwelling, which is common in deep-water slope and basinal facies, is considered the main cause of OM accumulation in these areas, as it delivers nutrients that significantly enhance primary productivity in surface waters (Mohialdeen & Hakimi, 2016; Al-Khatony et al., 2023). This is further supported by EF(Co) × EF(Mn), Co × Mn, and Cd/Mo values from several profiles (Fig. 7). Thus, the presence of upwelling events may account for the comparatively higher primary productivity in the basinal and deep-water slope facies (Fig. 8).

Enrichment mechanisms for organic matter

Sea level fluctuations, terrigenous inflow, and upwelling events are some of the processes that frequently influence the enrichment of organic matter (Robinson et al., 2022; Li et al., 2024; Liang et al., 2024). The effects of these events on organic matter enrichment vary depending on the geological setting, but they finally manifest as the regulation of primary productivity and the preservation of bottom water (Liu et al., 2017). Strong correlations between redox indices such as U/Th and TOC (R^2= 0.81, 0.64 for EB1 and Ba1, respectively) during the Late Jurassic–Early Cretaceous OSF1 and OSF2 deposition periods indicate that the primary bottom water conditions were anoxic and euxinic, providing ideal conditions for the preservation of organic matter. High primary productivity was maintained by nutrient input, and the deep-water slope and basin were connected to the open sea due to the relatively high sea level. This is consistent with the correlations shown by TOC (Fig. 6d & f), Ni/Co (R^2= 0.64, 0.46 and Cu/Al (R^2= 0.69, 0.37) for EB1 and Ba1, respectively. Therefore, higher organic matter accumulation and preservation are facilitated by the establishment of anoxic conditions and high productivity (Fig. 9a). The redox conditions during OSF4 deposition (in EB1 only) were regulated by relative sea level variations in the deep-water slope and basin (Al-Beyati, 1998). The comparatively high TOC values can be explained by intermittent euxinic and chronic anoxic conditions. When upwelling events were occurred, relatively high primary productivity consistently led to organic matter enrichment. As sea level gradually dropped throughout the OSF5 depositional period in the Late Jurassic–Early Cretaceous, progressive basin restriction led to decreased primary productivity and reduced nutrient supply. The main bottom water conditions simultaneously shifted from anoxic to suboxic, resulting in unfavourable conditions for organic matter preservation. Additionally, the diluting effect of increased terrigenous input on organic matter is shown by the lack of correlation between Ti/Al and TOC (R^2= 0.01, 0.2) for EB1 and Ba1, respectively (Wang et al., 2022) (Fig. 6g). The dilution by terrigenous input, low productivity, and relatively week reducing conditions therefore account for the low organic matter content in OSF5 (Fig. 9b).

The TOC value of OSF3 (0.5–1.9 wt. %, average 1.56 wt. % in EB1, and 0.39–1.57 wt. %, average 1.13 wt. % in Ba1) showed a recovery compared to OSF5, although it remains within a dysoxic environment. Fluctuation of the Ti/Al ratios, which indicate the influence of terrigenous input, may reflect a shift from an arid to a humid environment in the Iraqi sedimentary basin (Al-Beyati, 1998; Al-Khatony et al., 2023). This shift is also consistent with increasing Rb/Sr and decreasing Sr/Cu ratios (Fig. 3). Although this facies was deposited under regressive conditions as the basin became shallower, its moderate organic content, which is supported by relatively clastic rocks, may indicate the presence of primary productivity. The transport of organic matter into the basin is crucial for sustaining primary productivity and can help maintain it even under regressive conditions (Al-Beyati, 1998; Cox et al., 2016). Generally, the basin's extensive dysoxic to suboxic bottom water conditions are unfavourable for the preservation of organic matter, but this limitation has been partially offset by increased primary productivity and reduced terrigenous clastic input (Fig. 9c). These factors relate to the types of environments that predominated in the intra-

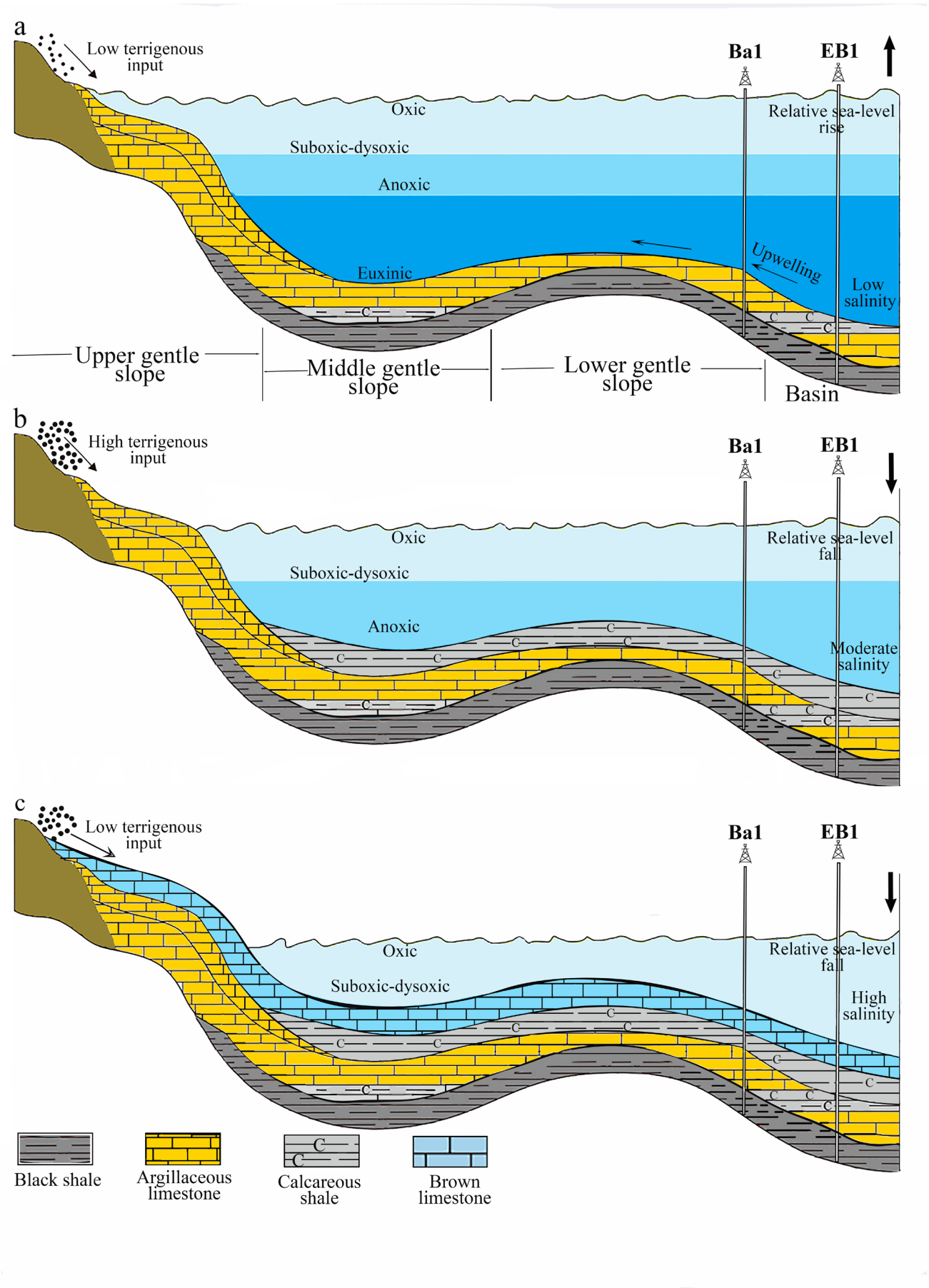

Fig. 9. Conceptual models illustrating organic matter accumulation in the Chia Gara Formation: (a) OSF1 and 2 – high primary productivity, and anoxic to euxinic bottom water conditions; (b) OSF3 – dysoxic bottom water conditions, low primary productivity, and high terrigenous input; (c) OSF4 and OSF5 – low terrigenous input, warm and humid environment, suboxic bottom water conditions, and moderately high primary productivity.

shelf basins on the northeastern margin of Arabian Plate (Jafarian et al., 2024). As the intra-shelf basins were located far from the equator, at the beginning of the Cretaceous period they were limited to latitudes 0–10° north and south, having been in the 0–30° south latitude range at the start of the Triassic. The stratified water conditions in a humid tropical climate during the Jurassic period of the Mesozoic were a distinctive and significant feature of the intra-shelf basins' environmental characteristics. At that time, these basins exhibited high productivity of organic material of kerogen type II, due to the stratified water conditions resulting from their distance from the equator (Wilson, 2020).

According to Sweere's (2016) analysis of several global regions, Cd/Mo ratios < 0.1 and Co × Mn > 0.4 indicate restricted basin locations driven by preservation conditions (e.g., Black Sea), whereas Cd/Mo ratios > 0.1 and Co × Mn < 0.4 indicate upwelling settings driven by productivity (e.g., Peruvian margin, Namibian margin) (Fig. 7b). The Cd/Mo ratios of the five organic sedimentary facies in this study show that most of OSF1, OSF2, and OSF4 sample points are located in the preservation area, while most of OSF3 and OSF5 samples are found in the productivity area. The significantly higher TOC values of the shales in OSF1, OSF2, OSF4, and OSF5 compared to those in OSF3 are consistent with this. Upwelling currents are considered to have a significant influence on organic matter enrichment. Although nutrient input is increased in the upwelling region, raising productivity, the decomposition of organic matter by anaerobic bacteria and plankton respiration also consume large amount of oxygen, resulting in an oxygen minimum zone that promotes organic matter enrichment (Sweere et al., 2016). Geological processes such as sea level rise, terrigenous inflow, and climatic change also affect organic matter enrichment, and their effects occur simultaneously (Algeo & Maynard, 2004).

Thus, preservation requirements are more important than productivity conditions in upwelling environments and are essential for the formation of high-quality hydrocarbon source rocks. Unlike other facies on the platform, such as the deep-water slope and basinal facies, which are predominantly driven by productivity, or the transitional facies, which are influenced by both productivity and preservation, the enrichment process in the intrashelf basin is very different.

Conclusions

The deep-water slope and basin in the East Baghdad and Balad Oilfields shifted from continuous anoxic-suboxic conditions. Intermittent euxinic to dysoxic bottom water settings occurred during the deposition of the Late Jurassic–Early Cretaceous Chia Gara Formation. The presence of euxinic conditions in this period is supported by the extremely redox-sensitive $\delta^{98/95}$Mo values in organic sedimentary facies 2 and 1. These values further clarify the redox setting of the bottom water at this time.

The TOC values of the lower organic sedimentary facies 1 (anoxic-suboxic) and 2 (euxinic) are higher than those of the upper organic sedimentary facies 3 (dysoxic), 4, and 5 (suboxic) in wells EB1 and Ba1. Primary productivity indices Cu/Al and Ni/Al ratios indicate that the average primary production level is relatively lower in the deep-water slope and basinal facies. Redox indicators such as EF(U), EF(Mo), Ni/Co, and U/Th show that bottom waters become more oxidised upwards. The terrigenous input proxy (Ti/Al) reflects the diluting effect of increased terrigenous input on organic matter. The upward increase in Rb/Sr and decrease in Sr/Cu indicate a climatic shift from hot and dry to warm conditions. The Mo/TOC ratio, a hydrographic indicator of the basin, demonstrates a strong connection between the basin and the open ocean.

The deep-water slope and basin show upwelling, as indicated by EF (Co) × EF (Mn) values ranging from 0 to 0.48 for EB1 and 0.05 to 0.18 for Ba1, which is in contrasts with other Arabian platform locations where no upwelling activity is observed. Upwelling events may explain the comparatively higher primary productivity of the basin facies. Primary productivity increased in organic sedimentary facies 3 and 5 after a gradual decline in facies 1, 2, and 4. Nutrient input sustained primary productivity, and the deep-water slope and basin were connected to the open sea due to the relatively high sea level.

The mechanisms underlying the enrichment of organic matter in the shale of the Chia Gara Formation differ among facies. In the lower part of the Chia Gara Formation within the Mesopotamian Fore Deep Basin (organic sedimentary facies, 2, and 4), preservation conditions have the greatest impact. In contrast, the upper part (organic sedimentary facies 3 and 5) is mainly influenced by productivity conditions. This indicates that preservation conditions are more important for organic matter enrichment in unrestricted environments with upwelling. This finding provides

valuable information for the investigation of the basin's high-quality hydrocarbon source rocks.

Acknowledgements

The core samples, data, and reports were supplied by the Midland Oil Company of Iraq (Md.O.C.), for which the authors are appreciative.

Formatting of funding sources

This research did not receive any specific grant from funding agencies in the public, commercial, or not-for-profit sectors.

Declaration of competing interest

The authors declare that they have no known competing financial interests or personal relationships that could have appeared to influence the work reported in this paper.

References

Abshire, M.L., Riedinger, N., Clymer, J.M., Scott, C., Severmann, S., Romaniello, S.J. & Puckette, J.O. 2021: Reconstructing the paleoceanographic and redox conditions responsible for variations in uranium content in North American Devonian black shales. Palaeogeography, Palaeoclimatology, Palaeoecology, 587, 110763. https://doi.org/10.1016/j.palaeo.2021.110763

Al-Ahmed, A.A.N. 2013: Determination and applications of chemical analysis to evaluate Jurassic hydrocarbon potentiality in Northern Iraq. Arab J. Geosci., 6: 2941–2949. https://doi.org/10.1007/s12517-012-0592-8

Al-Ameri, T.K. 2011: Khasib and Tannuma oil sources, East Baghdad oil field, Iraq. Marine and Petroleum Geology, 28/4: 880–894. https://doi.org/10.1016/j.marpetgeo.2010.06.003

Al-Ameri, T.K., Al-Nagshbandi, S., Al-Ahmed, A.A., Zumberge, J. & Pitman, J. 2012a: Middle and Upper Jurassic Palynostratigraphy and Hydrocarbon Potential in the Zagros Fold Belt, Northern Iraq. GEO-2012, 10th Middle East Geosciences Conference and Exhibition, 4–7 March 2012, Manama, Bahrain. American Association of Petroleum Geologists Search and Discovery Article #90141.

Al-Ameri, T.K. & Zumberge, J. 2012b: Middle and Upper Jurassic hydrocarbon potential of the Zagross Fold Belt, North Iraq. Marine and Petroleum Geology, 36: 13–34. https://doi.org/10.1016/j.marpetgeo.2012.04.004

Al-Ameri, T.K., Al-Temimi, A.K. & Zumberge, J. 2016: Assessments of oil characterization, source affinities, and hydrocarbon dynamic of East Baghdad oil fields, Central Iraq. Marine and Petroleum Geology, 77: 353–375. https://doi.org/10.1016/j.marpetgeo.2016.03.009

Al-Beyati, F.M.O. 1998: Organic geochemical and environmental evaluation study of Chia Gara Formation from selected boreholes in middle Iraq: Ph.D. dissertation (unpublished), College of Science, University of Baghdad, Baghdad, Iraq, 172 p.

Al-Beyati, F.M.O., Abdula, R.A. & Othman, R.S. 2021: Organic geochemistry of the Middle to Upper Jurassic source rocks succession in Balad-1 Well, Balad Oil Field, Central Iraq. Bull. Geol. Soc. Malays., 71: 125–138. https://doi.org/10.7186/bgsm71202111

Algeo, T.J. & Maynard, J.B. 2004: Trace-element behavior and redox facies in core shales of Upper Pennsylvanian Kansas-type cyclothems. Chemical Geology, 206/3–4: 289–318. https://doi.org/10.1016/j.chemgeo.2003.12.009

Algeo, T.J. & Maynard, J.B. 2008: Trace-metal covariation as a guide to water-mass conditions in ancient anoxic marine environments. Geosphere, 4: 872–887. https://doi.org/10.1130/GES00174.1

Algeo, T.J. & Tribovillard, N. 2009: Environmental analysis of paleoceanographic systems based on molybdenum–uranium covariation. Chem. Geol. 268: 211–225. https://doi.org/10.1016/j.chemgeo.2009.09.001

Algeo, T.J. & Li, C. 2020: Redox classification and calibration of redox thresholds in sedimentary systems. Geochim. Cosmochim. Acta, 287: 8–26. https://doi.org/10.1016/j.gca.2020.01.055

Ali, R.A. & Jassim, H.K. 2023: Sedimentology and geochemistry of Zubair Formation sandstone reservoir, East Baghdad Oilfield, central Iraq. Kuwait Journal of Science, 50/3: 427–437. https://doi.org/10.1016/j.kjs.2023.01.006

Ali, R.A. 2023: Petrography and geochemistry of Zubair Shale Formation in Rumaila Oilfield, Southern Iraq: Implications for provenance and tectonic setting. J. of Petroleum Research and Studies, 13/3. https://doi.org/10.52716/jprs.v13i3

Ali, M.A. 2018: Geochemical evaluation of organic matter in Jurassic source rocks, BEKHME-1 well, Erbil governorate, Kurdistan region, Iraq. Iraqi Bulletin of Geology and Mining, 14/2: 49–59.

Al-Jaafary, A.S.H. 2015: Mineralogy, Geochemistry and Oil Seepage Characteristics of Jurassic Rock Sequence (Sargelu, Naokelekan and Chia Gara Formations) at Zakho area/North Iraq.

Ph.D. dissertation (unpublished), College of Science, University of Baghdad, Baghdad, Iraq, 195 p.

Al-Khatony, F.H., AL-Hamidi, R.I. & Al-Lhaebi, S.F. 2023: Paleoenvironmental Conditions of the Chia Gara Formation from Rania Section North Eastern Iraq Using Geochemical Constraints. Iraqi National Journal of Earth Science, 23/1: 154–167. https://doi.org/10.33899/earth.2023.139987.1078

Chen, L., Chen, X., Tan, X., Zheng, J., Yang, Y., Jing, C., Zhou, H. & Wang, G. 2023: Factors controlling organic matter accumulation in the Longmaxi Formation shale, Changning area, South Sichuan Basin. Geomech. Geophys. Geo-energ. Geo-resour. 9: 89. https://doi.org/10.1007/s40948-023-00585-5

Cheng, M., Li, C., Zhou, L., Algeo, T.J., Zhang, F., Romaniello, S., Jin, C.S., Lei, L.D., Feng, L.J. & Jiang, S.Y. 2016: Marine Mo biogeochemistry in the context of dynamically euxinic mid-depth waters: A case study of the lower Cambrian Niutitang shales, South China. Geochim. Cosmochim. Acta, 183: 79–93. https://doi.org/10.1016/j.gca.2016.03.035

Cox, G.M., Jarrett, A., Edwards, D., Crockford, P.W., Halverson, G.P., Collins, A.S., Poirier, A. & Li, Z.-X. 2016: Basin redox and primary productivity within the Mesoproterozoic Roper Seaway. Chemical Geology, 440: 101–114. https://doi.org/10.1016/j.chemgeo.2016.06.025

Damoulianou, M-E., Perleros, K., Mohialdeen, I.M.J., Khanaqa, P., Araujo, C.V. & Kalaitzidis, S. 2022: Characterization of the bituminite-rich Chia Gara Formation in M-2 well Miran field, Kurdistan Region, NE Iraq. International Journal of Coal Geology, 263, 104115. https://doi.org/10.1016/j.coal.2022.104115

Edilbi, A.N.F. & Sherwani, G.H., 2019: Petrography and source rock potential of Chia Gara Formation (Late Jurassic–Early Cretaceous) in Northern Iraq and Kurdistan Region. J. pet. explor. prod. technol., 9: 1801–1818. https://doi.org/10.1007/s13202-019-0661-6

Gomes, M.L. & Hurtgen, M.T. 2015: Sulfur isotope fractionation in modern euxinic systems: Implications for paleoenvironmental reconstructions of paired sulfate–sulfide isotope records. Geochimica et Cosmochimica Acta,157: 39–55. https://doi.org/10.1016/j.gca.2015.02.031

Greber, N.D., Siebert, C., Nägler, T.F. & Pettke, T. 2012: δ98/95Mo values and molybdenum concentration data for NIST SRM 610, 612 and 3134: towards a common protocol for reporting Mo data. Geostand. Geoanal. Res. 36/3: 291–300. https://doi.org/10.1111/j.1751-908X.2012.00160.x

Hovikoski, J., Olivarius, M., Bojesen-Koefoed, J.A. & Piasecki, S. 2023: Late Jurassic – Early Cretaceous marine deoxygenation in Northeast Greenland. journal of the geological society, 180/3. https://doi.org/10.1144/jgs2022-058

Jafarian, A., Husinec, A., Wang, C., Chen, X., Wang, M., Gröcke, D.R., Saboor, A. & Li, Y. 2024: Intrashelf basin record of redox and productivity changes along the Arabian margin of Neo-Tethys during Oceanic Anoxic Event 1a. Palaeogeography, Palaeoclimatology, Palaeoecology, 636, 111975. https://doi.org/10.1016/j.palaeo.2023.111975

Jia, Z., Hu, Y., Bayon, G., Peckmann, J., Wang, X., Gong, S., Li, J., Roberts, H.H., Chen, D. & Feng, D. 2023: Seawater-fluid composition records from molybdenum isotopes of sequentially extracted phases of seep carbonate rocks. Geochemistry, Geophysics, Geosystems 24, e2023GC011128. https://doi.org/10.1029/2023GC011128

Jones, B. & Manning, D.A.C. 1994: Comparison of geochemical indices used for the interpretation of palaeoredox conditions in ancient mudstones. Chemical Geology, 111/1–4: 111–129. https://doi.org/10.1016/0009-2541(94)90085-X

Langrock, U., Stein, R., Lipinski, M. & Brumsack, H-J. 2003: Late Jurassic to Early Cretaceous black shale formation and paleoenvironment in high northern latitudes: Examples from the Norwegian-Greenland Seaway. Paleoceanography and Paleoclimatology, 18/3, https://doi.org/10.1029/2002PA000867

Lenstra, W., Seguret, M., Behrends, T., Groeneveld, R., Hermans, M., Witbaard, R. & Slomp, C.P. 2020: Controls on the shuttling of manganese over the northwestern Black Sea shelf and its fate in the euxinic deep basin. Geochimica et Cosmochimica Acta, 273. https://doi.org/10.1016/j.gca.2020.01.031

Liang, H., Wang, Z., Wang, J. & Wang, X. 2024: Organic Matter Enrichment in Jurassic Hydrocarbon Source Rocks from the Turpan-Hami Basin: Insights from Organic and Elemental Geochemistry. ACS Omega, 9/34: 36341-36352. https://doi.org/10.1021/acsomega.4c03367

Li, J., Liang, X. R., Zhong, L. F., Wang, X. C., Ren, Z. Y., Sun, S. L., Zhang, Z.F. & Xu, J.F. 2014: Measurement of the isotopic composition of molybdenum in geological samples by MC-ICP-MS using a novel chromatographic extraction technique. Geostandards and Geo-

analytical Research, 38/3: 345–354. https://doi.org/10.1111/j.1751-908X.2013.00279.x

Li, P., Liu, Z-B., Bi, H., Jiang, T., Bian, R-K., Wang, P-W. & Shang, X-Y. 2024: Differences in and factors controlling organic matter enrichment in the Ziliujing Formation shale in the Sichuan Basin. Petroleum Science, 21/1: 77–86. https://doi.org/10.1016/j.petsci.2023.10.020

Lin, D., Xi, Z., Tang, S., Lash, G.G., Guo, Q., Wang, H. & Zhu, Y. 2024: Organic matter enrichment in shale deposited proximal to paleo-uplifts and its impact on shale gas exploration. Palaeogeography, Palaeoclimatology, Palaeoecology, 633, 111900. https://doi.org/10.1016/j.palaeo.2023.111900

Liu, K., Feng, Q., Shen, J. & Khan, M.Z. 2017: Increased productivity as a primary driver of marine anoxia. Palaeogeography, Palaeoclimatology, Palaeoecology, 491. https://doi.org/10.1016/j.palaeo.2017.11.007

Lodowski, D.G., Szives, O., Virág, A. & Grabowski, J. 2024: The latest Jurassic–earliest Cretaceous climate and oceanographic changes in the Western Tethys: The Transdanubian Range (Hungary) perspective. Sedimentology, 71: 1843–1872. https://doi.org/10.1111/sed.13194

Lu, Y., Jiang, S., Lu, Y. & Xu, S. 2019: Productivity or preservation? The factors controlling the organic matter accumulation in the late Katian through Hirnantian Wufeng organic-rich shale, South China. Marine and Petroleum Geology, 109/3–4: 22–35. https://doi.org/10.1016/j.marpetgeo.2019.06.007

Lu, X., Dahl, T.W., Zheng, W., Wang, S. & Kendall, B. 2020: Estimating ancient seawater isotope compositions and global ocean redox conditions by coupling the molybdenum and uranium isotope systems of euxinic organic-rich mudrocks. Geochimica et Cosmochimica Acta, 290: 76–103. https://doi.org/10.1016/j.gca.2020.08.032

Lu, B., Hou, D-j., Zou, C-n., Li, X-z., Gao, R-s., Wei, H-y. & Qiu, Z. 2025: Depositional environment and organic matter enrichment mechanism of the lower cambrian shale in the southern Sichuan Basin. Front. Earth Sci. 13:1509332. https://doi.org/10.3389/feart.2025.1509332

McLennan, S.M. 2001: Relationships between the trace element composition of sedimentary rocks and upper continental crust. Geochemistry, Geophysics, Geosystems, 2. https://doi.org/10.1029/2000gc000109

McQuarrie, N. 2004: Crustal scale geometry of the Zagros fold thrust belt, Iran. Journ. Structural Geol., 26/3: 519–535. https://doi.org/10.1016/j.jsg.2003.08.009

Mohialdeen, I.M.J. & Raza, S.M. 2013: Inorganic geochemical evidence for the depositional facies associations of the Upper Jurassic Chia Gara Formation in NE Iraq. Arab J Geosci, 6: 4755–4770. https://doi.org/10.1007/s12517-012-0716-1

Mohialdeen, I.M.J. & Hakimi, M.H. 2016: Geochemical characterisation of Tithonian–Berriasian Chia Gara organic-rich rocks in northern Iraq with an emphasis on organic matter enrichment and the relationship to the bioproductivity and anoxia conditions. Journal of Asian Earth Sciences, 116: 181–197. https://doi.org/10.1016/j.jseaes.2015.11.004

Mustafa, R.K. & Tobia, F.H. 2020: Geochemical application in unraveling paleo weathering, provenance and environmental setting of the shale from Chia Gara Formation, Kurdistan Region, Iraq. Iraqi Geological Journal, 53:1A. https://doi.org/10.46717/igj.53.1a.R7.2020.01.28

Nan, J., Tsang, M.-Y., Li, J., Köster, M., Henkel, S., Lin, F. & Yao, W. 2023: Postdepositional behavior of molybdenum in deep sediments and implications for paleoredox reconstruction. Geophysical Research Letters, 50, e2023GL104706. https://doi.org/10.1029/2023GL104706

Nagler, T., Pierau, N., Böttcher, M.E., Dellwig, O. & Schnetger, B. 2011: Molybdenum isotope fractionation in pelagic euxinia: Evidence from the modern Black and Baltic Seas. Chemical Geology, 289/1–2: 1–11. https://doi.org/10.1016/j.chemgeo.2011.07.001

Okuyama, A., Kashiwabara, T., Kurisu, M., Takahashi, Y. & Fukushi, K. 2025: Effect of manganese oxide mineralogy and surface Mo coverage on Mo isotope fractionation during the adsorption process. Minerals, 15/1: 79. https://doi.org/10.3390/min15010079

Pearce, C.R., Coe, A.L. & Cohen, A.S. 2010: Seawater redox variations during the deposition of the Kimmeridge Clay Formation, United Kingdom (Upper Jurassic): Evidence from molybdenum isotopes and trace metal ratios. Paleoceanography, 25, PA4213. https://doi.org/10.1029/2010PA001963, 2010

Ritzer, S.R., Schoepfer, S., Bussian, B., Farrell, U.C., Fraser, T., Henderson, C.M., Kang, J., Mwinde, C.N., Patch, A. & Sperling, E.A. 2024: The relationship between total organic carbon and bottom water redox state in North American black shales. Palaeogeography, Palaeoclimatology, Palaeocology, 649, 112266. https://doi.org/10.1016/j.palaeo.2024.112266

Robinson, L.J. & Whiteside, J.H. 2022: Models of organic enrichment in epicontinental basins: Applications of a large organic geochemical dataset from the Cretaceous Western Interior Seaway. Cretaceous Research, 134, 105160. https://doi.org/10.1016/j.cretres.2022.105160

Schoepfer, S.D., Shen, J., Wei, H., Tyson, R.V., Ingall, E. & Algeo, T.J. 2015: Total organic carbon, organic phosphorus, and biogenic barium f luxes as proxies for paleomarine productivity. Earth Sci. Rev., 149: 23–52. https://doi.org/10.1016/j.earscirev.2014.08.017

Shen, J.-J., Yan, J.-K., Wang, P.-W., Wang, Y.-M., Zhou, L., Ji, Y.-B., Xu, M. 2024: Upwelling current and its relationship to the enrichment of organic matter in the Lower Silurian Longmaxi Formation, northern Chongqing–western Hubei area, southern China. Journal of Paleogeography, 13/4: 993–1015. https://doi.org/10.1016/j.jop.2024.08.005

Shi, J., Zou, Y-R., Cai, Y-L., Zhan, Z-W., Sun, J-N., Liang, T. & Peng, P. 2022: Organic matter enrichment of the Chang 7 member in the Ordos Basin: Insights from chemometrics and element geochemistry. Marine and Petroleum Geology, 135, 105404. https://doi.org/10.1016/j.marpetgeo.2021.105404

Siebert, C., Nagler, T.F. & Kramers, J.D. 2001: Determination of Molybdenum Isotope Fractionation by Double-Spike Multicollector ICPMS. Geochem. Geophys. Geosyst. 2, https://doi.org/10.1029/2000GC000124

Simmons, M.D., Sharland, P.R., Casey, D.M., Davies, R.B. & Sutcliffe, O.E. 2007: Arabian Plate sequence stratigraphy: Potential implications for global chronostratigraphy. GeoArabia, Gulf PetroLink, Bahrain, 12/4: 101–130. https://doi.org/10.2113/geoarabia1204101

Sweere, T., Boorn, S.V.D., Dickson, A.J. & Reichart, G-J. 2016: Definition of new trace-metal proxies for the controls on organic matter enrichment in marine sediments based on Mn, Co, Mo and Cd concentrations. Chem. Geol., 441: 235–245. https://doi.org/10.1016/j.chemgeo.2016.08.028

Taylor, S. R. & McLennan, S.H. 1985: The geochemical evolution of the continental crust. Review Geophysics, 33: 241–265. https://doi.org/10.1029/95RG00262

Tribovillard, N., Algeo, T.J., Lyons, T. & Riboulleau, A. 2006: Trace metals as paleoredox and paleoproductivity proxies: An update. Chem. Geol., 232: 12–32. https://doi.org/10.1016/j.chemgeo.2006.02.012

Tribovillard, N., Algeo, T.J., Baudin, F. & Riboulleau, A. 2012: Analysis of marine environmental conditions based on molybdenum uranium covariation—Applications to Mesozoic paleoceanography. Chem. Geol., 324–325:46–58. https://doi.org/10.1016/j.chemgeo.2011.09.009

Tsujisaka, M., Takano, S., Murayama, M. & Sohrin, Y. 2019: Precise analysis of the concentrations and isotopic compositions of molybdenum and tungsten in geochemical reference materials. Analytica Chimica Acta, 1091: 146–159. https://doi.org/10.1016/j.aca.2019.09.003

Vorlicek, T.P., Helz, G., Chappaz, A. & Vue, P. 2018: Molybdenum Burial Mechanism in Sulfidic Sediments: Iron-Sulfide Pathway. ACS Earth and Space Chemistry. 2/6. https://doi.org/10.1021/acsearthspacechem.8b00016

Wang, Z., Shen, L., Wang, J. & Fu, X. 2022: Organic matter enrichment of the Late Triassic Bagong Formation (Qiangtang Basin, Tibet) driven by paleoenvironment: Insights from elemental geochemistry and mineralogy. Journal of Asian Earth Sciences, 236/3–4:105329. https://doi.org/10.1016/j.jseaes.2022.105329

Wang, S., Dong, T., He, Z., Guo, X. & Liu, S. 2024: Hydrographic restriction conditions in the Middle and Upper Yangtze region during the Early Silurian post-glacial transgression: Constraints from major, trace elemental geochemistry and Mo-TOC relationship. Palaeogeography, Palaeoclimatology, Palaeocology, 655, 112546. https://doi.org/10.1016/j.palaeo.2024.112546

Wilson, A.O. 2020: Introduction to the Jurassic Arabian Intrashelf Basin. Geological Society London Memoirs, 53/1: 1–19. https://doi.org/10.1144/M53.1

Zhang, Q., Liu, E., Pan, S., Wang, H., Jing, Z., Zhao, Z. & Zhu, R. 2023: Multiple Controls on Organic Matter Accumulation in the Intraplatform Basin of the Early Cambrian Yangtze Platform, South China. J. Mar. Sci. Eng., 11/10. https://www.mdpi.com/2077-1312/11/10/1907#

Zhao, P.P., Li, J., Zhang, L., Wang, Z.B., Kong, D.X., Ma, J. L., Wei, G.J. & Xu, J.F. 2016: Molybdenum mass fractions and isotopic compositions of international geological reference materials. Geostandards and Geoanalytical Research, 40/2: 217–226. https://doi.org/10.1111/j.1751-908X.2015.00373.x